N A S A Contractor Report

N O N - I N T R U S I V E F L O W M E A S U R E M E N T S

O N A R E - E N T R Y V E H I C L E

(NASA-CR-169959) NON-INTRUSIVE FLOW MEASUREMENTS ON A REENTRY VEHICLE Final Report, 26 Jan. 1982 - 25 Jan. 1983 (Princeton Univ., N. J.) 84 p HC A05/MF A01 CSCL 01A G3/02

N83-18670

Unclas 02926

R. B. Miles, D. A. Santavicca and M. Zimmermannn
Princeton University
Princeton, New Jersey

Prepared for
NASA Langley Research Center
under Contract NCCI-64

TECHNICAL REPORT STANDARD TITLE PAGE

1. Report No.	2. Government Accession No.	3. Recipient's Catalog No.

4. Title and Subtitle	5. Report Date
NON-INTRUSIVE FLOW MEASUREMENTS ON A RE-ENTRY VEHICLE	February 16, 1983
	6. Performing Organization Code
7. Author(s)	8. Performing Organization Report No.
R.B. Miles, D.A. Santavicca, & M. Zimmermann	
9. Performing Organization Name and Address	10. Work Unit No.
Department of Mechanical and Aerospace Engineering Princeton University, Princeton, NJ 08544	11. Contract or Grant No. NCC1-64
	13. Type of Report and Period Covered Final Report 1/26/82 - 1/25/83
12. Sponsoring Agency Name and Address Langley Research Center Hampton, VA 23665	14. Sponsoring Agency Code NASA

15. Supplementary Notes

16. Abstract

This study evaluates the utility of various non-intrusive techniques for the measurement of the flow field on the windward side of the Space Shuttle or a similar re-entry vehicle. Included are linear (Rayleigh, Raman, Mie, Laser Doppler Velocimetry, Resonant Doppler Velocimetry) and nonlinear (Coherent Anti-Stokes Raman, Laser Induced Fluorescence) light scattering, electron beam fluorescence, thermal emission and mass spectroscopy. Flow field properties are taken from a nonequilibrium flow model by Shinn, Moss and Simmonds at NASA Langley. Conclusions are, when possible, based on quantitative scaling of known laboratory results to the conditions projected. Detailed discussion with researchers in the field contributed further to these conclusions and provided valuable insights regarding the experimental feasibility of each of the techniques.

17. Key Words (Selected by Author(s))	18. Distribution Statement
Re-entry, Nonintrusive Diagnostics, Space Shuttle, Shuttle Flow Field, Rayleigh Scattering, Raman Scattering, Mass Spectroscopy, Laser Induced Fluorescence	

19. Security Classif. (of this report)	20. Security Classif. (of this page)	21. No. of Pages	22. Price*
UNCLASSIFIED	UNCLASSIFIED	80	

*For sale by the Clearinghouse for Federal Scientific and Technical Information, Springfield, Virginia 22151.

Figure 2. Technical Report Standard Title Page

TABLE OF CONTENTS

LIST OF FIGURES

LIST OF TABLES

NON-INTRUSIVE FLOW MEASUREMENTS ON A RE-ENTRY VEHICLE

R. B. Miles, D. A. Santavicca, and M. Zimmerman

Abstract

This study evaluates the utility of various non-intrusive techniques for the measurement of the flow field on the windward side of the Space Shuttle or a similar re-entry vehicle. Included are linear (Rayleigh, Raman, Mie, Laser Doppler Velocimetry, Resonant Doppler Velocimetry) and nonlinear (Coherent Anti-Stokes Raman, Laser Induced Fluorescence) light scattering, electron beam fluorescence, thermal emission and mass spectroscopy. Flow field properties are taken from a nonequilibrium flow model by Shinn, Moss and Simmonds at NASA Langley. Conclusions are, when possible, based on quantitative scaling of known laboratory results to the conditions projected. Detailed discussion with researchers in the field contributed further to these conclusions and provided valuable insights regarding the experimental feasibility of each of the techniques.

NON-INTRUSIVE FLOW MEASUREMENTS ON A RE-ENTRY VEHICLE

1. Introduction

This project was undertaken to determine which if any of a variety of nonintrusive diagnostic techniques might be useful in determining flow properties on the windward side of a re-entering Space Shuttle or a separate re-entry vehicle. Our procedure was to first estimate the detection capabilities of the techniques at conditions corresponding to those expected in the flow field surrounding the Space Shuttle as it passes between 80 and 40 km in altitude. Where possible we used existing experimental results and extrapolated to the desired conditions. In some of these estimates we were guided by ongoing work in our own laboratories and in others by results published in the literature. Subsequently a presentation was made to the Princeton Advisory Group and the relative merits of each technique, plus a list of the important parameters to be measured were discussed. In order to further explore the promises and limitations of each of the techniques, a wide variety of researchers were visited and detailed discussions undertaken. These included trips to NASA Langley, United Technologies, NASA Ames, University of California-Berkeley, Sandia-Livermore Laboratories, and Stanford University. This provided us with an opportunity to learn the state-of-the-art in each of the areas and to obtain specific comments and perceptions from these researchers with regard to the potential of each of the techniques. Where relevant many of these comments are included in the appendices in which the techniques are discussed in detail.

2. Summary of the Results

The flow field conditions which were used in this study were largely taken from work conducted at NASA Langley by J. L. Shinn, J. N. Moss and A. L. Simmonds.[1] Figures 1 and 2 show plots of velocity, density and temperature for a re-entering Shuttle at altitudes of 74.95 km and 52.43 km, respectively. Each is shown as a function of the distance from the wind-ward surface at two points along the centerline. Here, the calculation is done for an equivalent hyperboloid whose parameters are determined by the pitch angle of the re-entering vehicle. The arrows indicate the conditions at the wall assuming a finite catalytic activity. The free stream conditions and equivalent body parameters are given in Table 1.[2] Each of the curves in Figures 1 and 2 terminates at the shock boundary and thereafter the free stream conditions apply.

These calculated results depend strongly on the effects of nonequilibrium heating and surface catalytic activity. For example, Figures 3 and 4 show calculated values of species mass fractions at 75 km altitude assuming in Figure 3 a non-catalytic wall and in Figure 4 a fully or equilibrium catalytic wall. Depending on the range in catalytic activity, the wall temperature can vary by over 30%. In Figures 3 and 4 note that there is a large change in the species concentration near the wall with a large NO concentration indicating strong catalytic effects. At low altitudes the temperature behind the shock is too low to produce significant radical concentrations (Figure 5).[3] These species and temperature distributions behind the shock depend strongly on estimates of reaction rates. Consequently, the validity of the model remains largely unknown until temperature profiles or species profiles can be measured. Density and velocity profiles

Figure 1. Velocity, temperature and density outward from the windward centerline of the re-entering Space Shuttle at an altitude of 74.95 km. Conditions are shown for two locations (s*): 1.2 meters from the nose ($s/R_N = .9$) and 33.5 meters from the nose ($S/R_N = 25$) [Ref. 1].

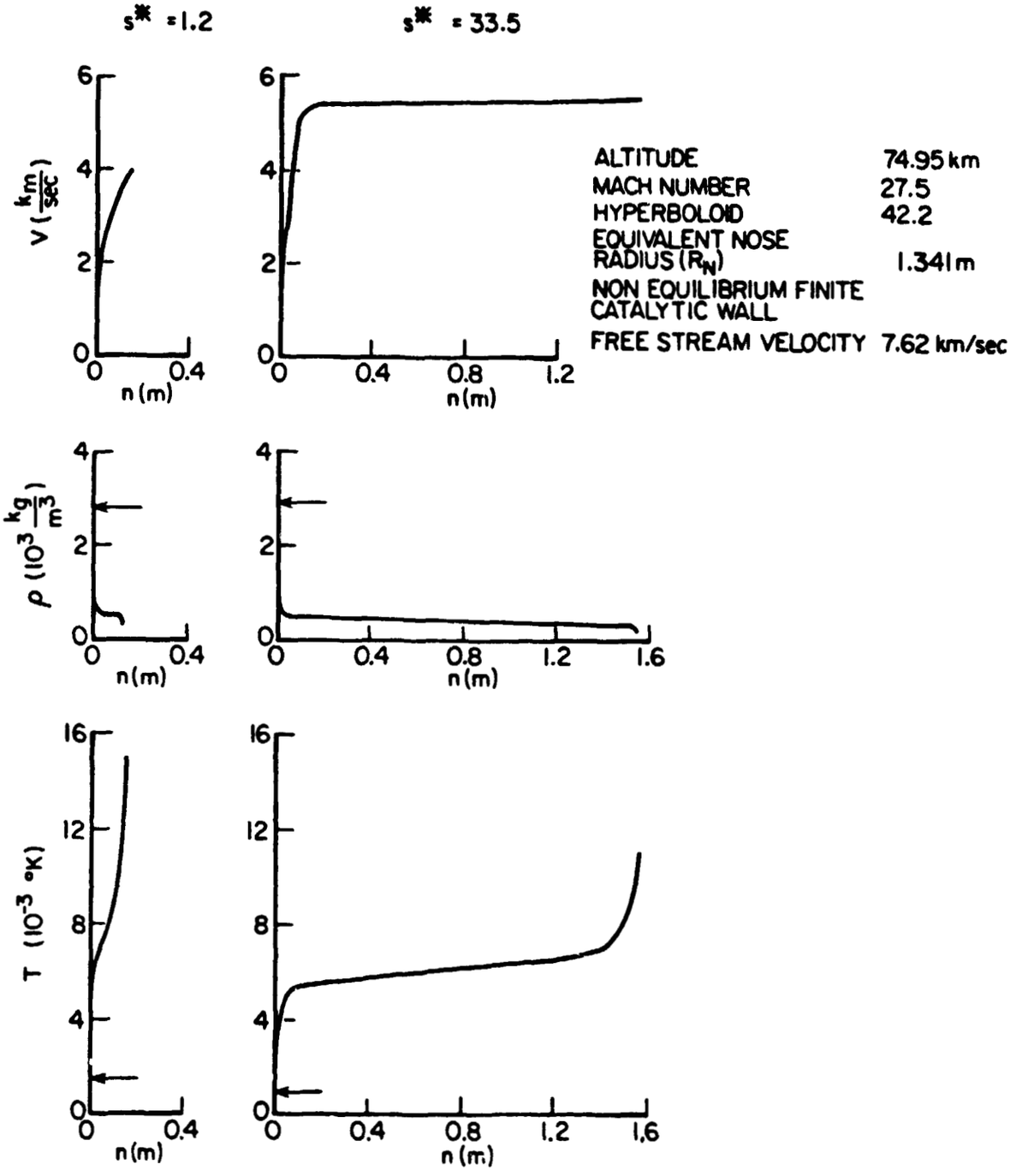

Figure 2. Velocity, temperature and density outward from the windward centerline of the re-entering Space Shuttle at an altitude of 52.43 km. Conditions are shown for two locations (s*): 1.1 meters from the nose ($s/R_N = .9$) and 30.8 meters from the nose ($s/R_N = 25$) [Ref. 1].

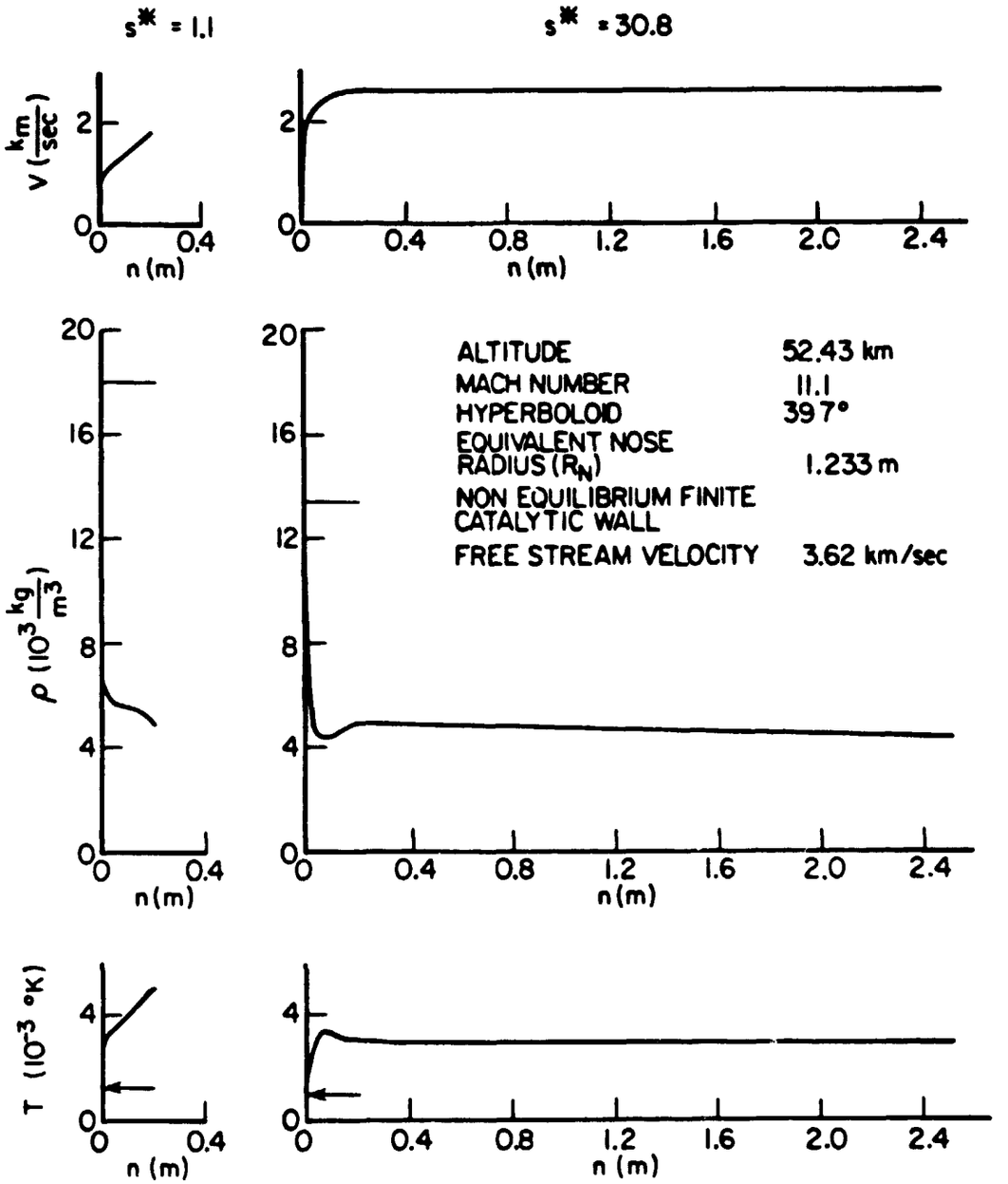

Figure 3. Species mass fraction for nonequilibrium flow with a non-catalytic wall [Ref. 1]. (42.2° Hyperboloid; $R_N = 1.34$ m; $s/R_N = 10.0$; Alt = 74.98; $M_\infty = 27.5$; $T_w = 1500°K$).

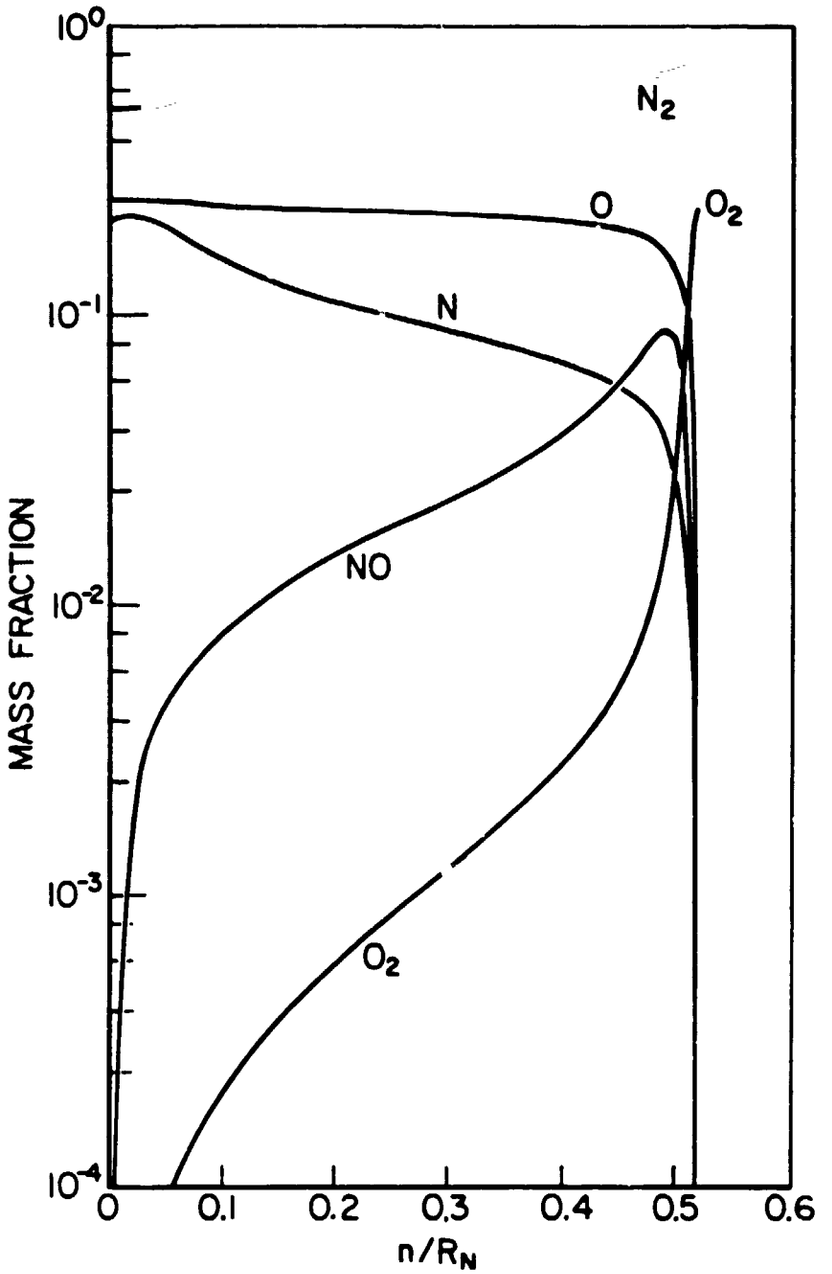

Figure 4. Species mass fraction for nonequilibrium flow with an equilibrium catalytic wall [Ref. 1]. (42.2° Hyperboloid; $R_N = 1.341$ m; $s/R_N = 10.0$; Alt = 74.98; $M_\infty = 27.5$; $T_w = 1500°K$).

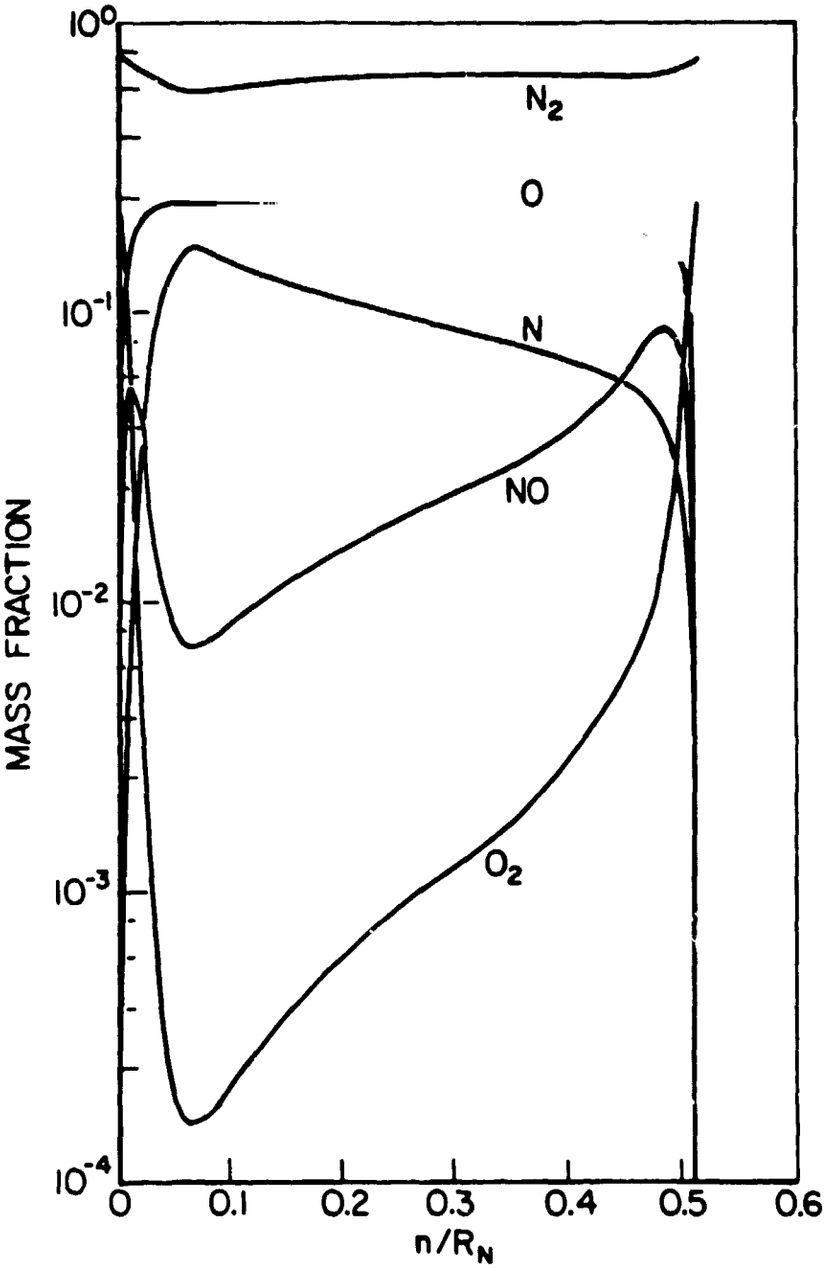

Figure 5. Species mass fraction for nonequilibrium flow with a finite catalytic wall [Ref. 3]. Alt = 156.5 ft (47.67 km); M = 9.15; $\alpha = 34.8°$; $s/R_N = 25$.

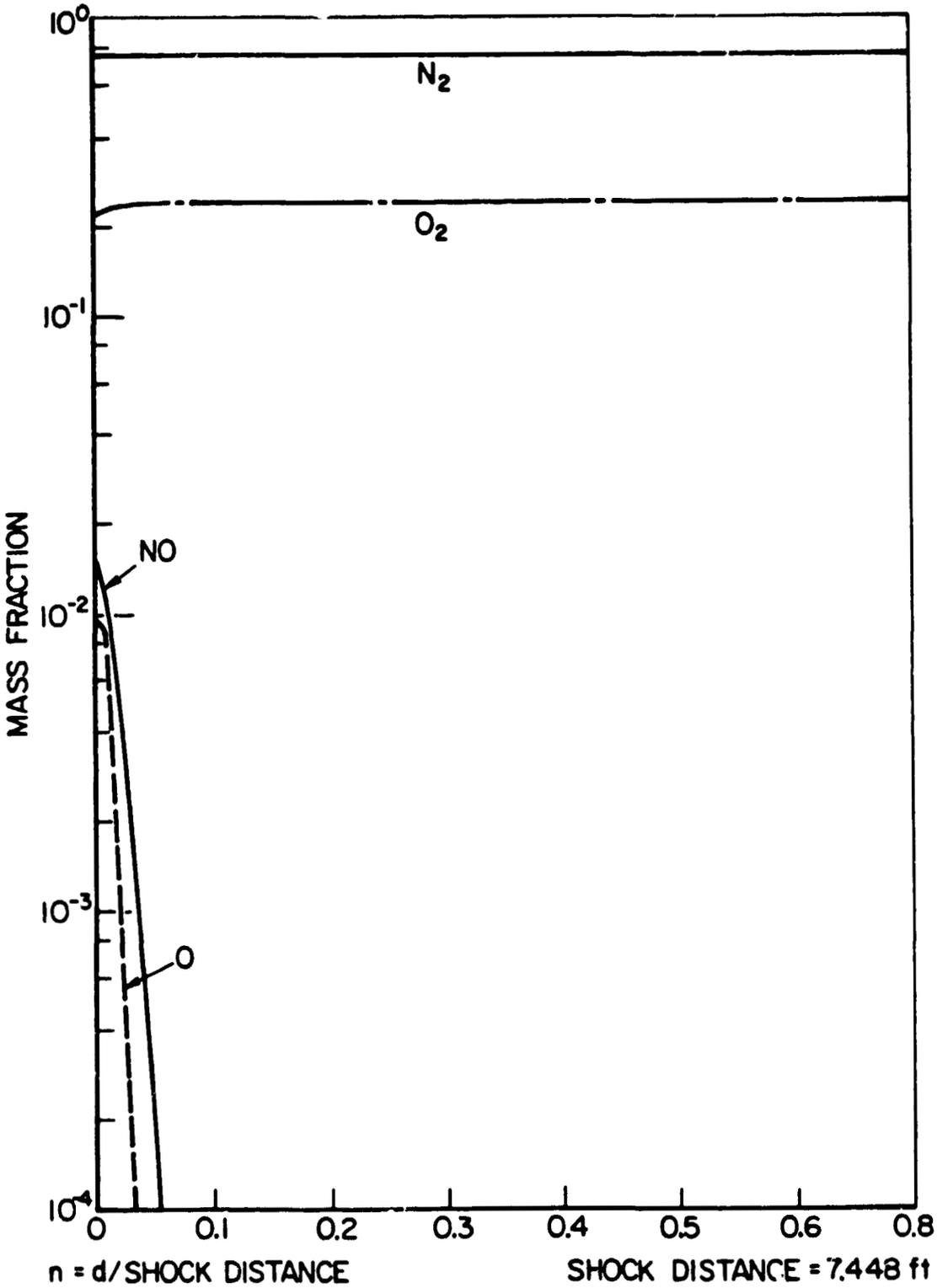

Table 1. Freestream conditions and equivalent body parameters.[2]

Case	Altitude, km	u_∞, km/sec	ρ_∞, kg/m^3	M_∞	α	Equivalent Body* θ	Equivalent Body* R_N, m
1	74.98	7.62	3.80×10^{-5}	27.5	41.4	42.20	1.341
2	68.88	6.61	9.28×10^{-5}	22.6	40.2	40.85	1.286
3	64.92	5.94	1.55×10^{-4}	19.6	34.5	35.20	1.042
4	60.66	5.12	2.61×10^{-4}	16.4	31.8	32.40	.938
			STS-1 Conditions				
5	52.43	3.62	7.43×10^{-4}	11.1	39.0	39.7	1.233
6	48.16	2.98	1.33×10^{-3}	9.15	34.8	35.4	1.052
7	44.04	2.30	2.40×10^{-3}	7.14	30.9	31.6	.908

α angle of attack

* Hyperboloid with body half angle θ and nose radius R_N at zero degree angle of attack.

as well as the location of the shock are also of significant interest. Near the nose the shock stands less than 20 cm from the surface and substantial variations in velocity, temperature, density and species concentrations occur over a few millimeters. These gradients are largest through the boundary layer where phenomena most directly related to the surface will occur.

The capabilities of the various nonintrusive detection methods are shown in Table 2. This table breaks the techniques into three categories. The first includes passive techniques which do not require illumination of the flow. Thermal emission naturally occurs from hot gases and particles and may be collected through a window and analyzed by an optical spectrometer. Mass spectroscopy involves sampling at the surface and subsequent analysis of gas constituents. The second category includes techniques which require actively probing the flow field with light or an electron beam. The last category includes techniques which require both active probes and a foreign species seeded into the flow field. Note that, in theory, numerous ways are available for measuring both temperature and species concentrations.

The selection of the flow properties which would be the most valuable to measure was a topic of substantial discussion. Clearly one would like to measure everything. Almost any measurement would give some check on the accuracy of the modelling. It was generally agreed however that species concentration or temperature would be especially useful as a check of the model. Certainly a profile of one of these two variables would produce data of substantial interest. This is not to neglect the importance of the density profile, shock location, velocity profile or the measurement of free stream conditions. One of the most common concerns raised was the density of particles and the amount of thermal emission encountered in the flow.

Table 2
Capabilities of Nonintrusive Detection Methods

	TECHNIQUE	MEASUREMENT				
I.	Mass Spectroscopy		Species Concentration			
	Thermal Emission	Temperature	Species Identity			
II.	Rayleigh Scattering	Temperature		Density	Velocity	
	Raman Scattering	Temperature	Species Concentration			
	Coherent Anti-Stokes Raman Scattering - CARS	Temperature	Species Concentration	Density		
	Mie Scattering					Particle Size/Density
	Laser Induced Fluorescence	Temperature	Species Concentration			
	Electron Beam Fluorescence	Temperature	Species Concentration			
III.	Laser Doppler Velocimetry				Velocity	Particle Size/Density
	Resonant Doppler Velocimetry	Temperature		Density	Velocity	

These two questions clearly affect the viability of several of the techniques and should be answered at an early stage. As will be evident in the following discussion, species measurements will be the most difficult to obtain with existing techniques. On the other hand, density profiles, temperature profiles, velocity profiles, particulate profiles, and the shock location may well be achievable with current technology.

A detailed discussion of each of the techniques and the methodology used for evaluation is presented at the end of this report. Table 3 is a summary of the conclusions. This table is broken into five categories. The first includes techniques which have undergone substantial laboratory testing and appear to have high promise. These are Rayleigh scattering, especially for density measurements and potentially for temperature and velocity measurements, and Mie scattering for particle concentrations, velocity and size. The second category includes techniques which also appear promising but have either not been adequately demonstrated in the laboratory or their success depends strongly on the magnitude of the background noise levels. These are laser induced fluorescence measurements of N, O and NO concentrations and temperature (from NO), and mass spectroscopy. Laser induced fluorescence may produce profiles of the N, O or NO concentrations which are sensitive indicators of the chemistry at high altitudes. Mass spectroscopy may be capable of determining species concentrations within the boundary layer throughout re-entry. The third category includes techniques which will require substantial additional work and are of questionable utility. These are quantitative thermal emission, electron beam fluorescence, and spontaneous Raman scattering measurements of temperature and concentration. The fourth category includes techniques which appear to have very little promise.

Table 3.
Summary of Conclusions

CATEGORY	TECHNIQUE	PROJECTION
1	A. Rayleigh Scattering	Very Promising
	B. Mie Scattering	Very Promising
2	C. Laser Induced Fluorescence	Promising
	D. Mass Spectroscopy	Promising
3	E. Thermal Emission	Needs More Research
	F. Electron Beam Fluorescence	Needs More Research
	G. Raman Scattering	Needs More Research
4	H. Coherent Anti-Stokes Raman Scattering - CARS	Little Promise
5	I. Laser Doppler Velocimetry	Require Seeding
	J. Resonant Doppler Velocimetry	Require Seeding

The only technique in this category is coherent anti-Stokes Raman scattering where the low densities, high temperature and crossed-beam phase-matching result in low signal strengths. A fifth category is reserved for those techniques which require seeding. It is currently impossible to determine the promise of these techniques, however it may be possible to use ablated material or naturally occurring particles in such a manner that the techniques may be viable. These are laser Doppler velocimetry and resonant Doppler velocimetry. Each of the techniques is further discussed in its associated appendix.

In our estimation the most promising technique is Rayleigh scattering. This has been demonstrated in the laboratory to be capable of measuring density and temperature. The scattering is observed at the same frequency as the laser and therefore the signal is subject to substantial noise interference from scattering from particies which may be in the flow stream. Similarly, observations very close to the window may be difficult due to background light scattered from the window itself. Various species have different Rayleigh scattering cross sections. These do not vary substantially from that of N_2, and, since N_2 is always the major species, its cross section may be used for density and velocity measurements. For temperature measurements, however, the different molecular weights of the different species will cause different broadening of the scattered light, somewhat complicating the measurement. The Rayleigh technique involves a single laser probe and could use an array of detectors so that a single laser pulse would yield an entire profile. It has been demonstrated in the laboratory that such a system may be integrated with a Mie scattering system for the detection of particulates. For example, when light is strongly scattered

from a particle, simple logic in the detection system may be used to exclude that signal from the Rayleigh scattering measurement and separately register it in a particle counter. Thus a single apparatus may conceivably yield pressure, temperature, velocity and particulate profiles.

We also find laser induced fluorescence from O, N and NO to be a promising technique for both concentration and temperature measurements. This has not yet been fully demonstrated in the laboratory under conditions which can easily be related to the re-entry environment. Therefore we must include this technique in the second category. Our enthusiasm is based on the importance of these species as an indicator of the nonequilibrium chemical dynamics, particularly at high altitude. Although there are difficulties in using this technique to measure species concentrations, the wide range of species densities behind the shock should nonetheless be observable. The work of McKenzie et al. at NASA Ames has been largely directed towards the use of this technique for temperature measurements. Using the technique as he has done, it would appear that temperature profiles may be obtainable using two sequential laser pulses of different wavelengths. With this technique we also note that scattering may be observed by multiple detectors as was true of Rayleigh scattering so that a profile may simultaneously be taken. Since a pulsed laser is used and fluorescence is observed over a rather narrow range of the spectrum, thermal emission can largely be excluded.

Our evaluation of mass spectroscopy was limited since no operational system for extracting the gas sample through the vehicle surface has yet been developed. There are two serious limitations associated with this technique. The first is that it samples from an area in such close proximity to the sampling port that it may not be indicative of the conditions

at the surface at all. This will particularly be true if the sampling port is large in the streamwise direction. The second problem is that the sample gas in passing through the sampling probe will most certainly undergo recombination and as such will not be truly indicative of the species concentrations in the boundary layer. Discussions with Dr. William McLean at Sandia and Drs. Daniel Seery and Med Colket of United Technologies indicate that a scavenging probe may be useful to alleviate this problem. For example, one could introduct hydrogen at the sampling port to interact with the oxygen atoms or O_{18} to interact with nitrogen atoms to produce a stable species that would in effect tag the original species. A similar idea is being studied by George Wood at NASA Langley using isotopic labelling on the wall material. This technique was originally suggested by Fristrom[4] and is currently being used for radical species diagnostics in combustion. With proper care in the design of the intake port and a careful selection of pumping rates, this may be an effective way of doing species identification in close proximity to the surface.

Although thermal emission and electron beam fluorescence may have the capability of yielding temperature and species concentrations, they are both better used for qualitative than quantitative study of the flow field. For example thermal emissions might enable one to determine the total column density which could then be used with laser induced fluorescence to correct for trapping effects as has been suggested by Professor John Daily of the University of California. The thermally emitted light must be collected over an integrated path and therefore point measurements will be difficult if not impossible. Pressure and temperature effects will further confuse the analysis. Similarly electron beam fluorescence has been developed as a

flow visualization tool and is not well adapted to quantitative measurements under these conditions. As Dr. William Hunter of NASA Langley pointed out, both quenching and temperature effects are not well understood. The electron beam does have the advantage however that it will operate at very high altitudes and might be useful as a qualitative density probe for the low densities encountered in the early stages of re-entry.

The quantum noise limited sensitivity estimates for spontaneous Raman predict that N, O, NO, O_2 and N_2 concentration measurements and N_2 vibrational temperature measurements should be possible over the entire range of altitudes. This is encouraging but perhaps misleading since the smallest amount of background noise from thermal emission or laser induced particulate incandescence will render this technique useless. Until more information is available about the thermal emission and particle density conditions however it is reasonable to keep Raman scattering under consideration.

Coherent anti-Stokes Raman scattering was found to be incapable of providing useful information under these conditions. The combination of low density, high temperature and short interaction length (because of the required crossed beam phase matching) lead to a signal strength below the detection limit. It is also restricted to single point measurements and, because of the required wide angle crossed beam phase matching, it would be very difficult to measure profiles unless a tremendous amount of experimental complexity were involved.

If the flow field could be seeded either from the surface of the vehicle or by a cloud of seed material, then several other techniques become available. In particular, laser doppler velocimetry (LDV) may be an attractive way of measuring velocity profiles. Due to the very high velocities,

however, conventional LDV configurations are not appropriate. Several alternatives may be considered including a simple monitoring of the transit time scattering intensity profile as a particle passes through a single light beam as has been discussed by Dr. Don Holve of Sandia-Livermore, or the use of interferometers to observe the large spectral shifts off the light scattered by rapidly moving particles. Another possibility is the crossing of two collimated laser beams at a very slight angle to produce widely spaced interference fringes to lower the modulation frequency of the fast particles passing through the laser beams. In this case the depth of field becomes large and a multiple detector system may be able to observe the velocity profile.

Similarly if sodium atoms could be seeded into the flow, then the resonant Doppler velocimeter could be used to measure temperature, density and velocity. This technique requires that the laser frequency be scanned and thus integration times of a few seconds would be expected. Here again an array of detectors can simultaneously observe the entire flow field profile. Using this technique the velocity profiles should be easily discernible, however quenching effects and the wide range of temperatures may lead to difficulty with the temperature and density measurements.

3. Recommendations

Throughout this study many questions were raised concerning the density of particulates and the amount of thermal emission on the windward side of the re-entry vehicle. It should be clear that the density of particulates is an extremely important quantity since it provides both a noise source and a potential seed source for laser Doppler velocimetry. In the case of Raman scattering even relatively low levels of thermal emission or low densities

of particles will prohibit its use. Clearly if the number of particulates is exceptionally high, it may also obscure the Rayleigh scattering or the laser induced fluorescence signals and eliminate laser Doppler velocimetry as an effective diagnostic tool. On the other hand, if the number of particulates is low, Rayleigh scattering may be viable and might be used for temperature and velocity as well as density measurements, but laser Doppler velocimetry may not be possible. Similarly, thermal emission, if excessive, may obscure the laser induced fluorescence signal as well as Rayleigh scattering. For these reasons we recommend that a preliminary experiment be planned to measure the particle density and thermal emission. This could be done using a simple laser beam and through a window collecting the Mie scattering at the laser frequency and the broad band thermal emission. As previously mentioned, this could be integrated with a Rayleigh scattering experiment if proper signal processing was done. With this information, preliminary estimates of the particle density and thermal emission intensity could be made and perhaps a density profile found.

Our results indicate that Rayleigh and Mie scattering and laser induced fluorescence are promising techniques. We would like to recommend that further work be undertaken on the development of these techniques with this particular application in mind. With regard to mass spectroscopy, our conclusion is that the technique has promise but is as yet unproven. It would appear that a measurement of species concentrations would require the use of a reacting tag, either in the gas phase, or on the surface of the probe. The major limitation of this technique is its inability to probe beyond the surface and the possibility that the catalytic nature of the entrance port may perturb the species concentrations from what would normally be encountered along the vehicle surface.

References

1. Shinn, J.L., Moss, J.N. and Simmonds, A.L., 1982, "Viscous-Shock-Layer Laminar Heating Analysis for the Shuttle Windward-Symmetry Plane with Surface Finite Catalytic Recombination Rates," AIAA/ASME Joint Fluids, Plasmas, Thermophysics and Heat Transfer Conference, June 7-11, 1982, St. Louis, Missouri.

2. Scott, D.C., 1981, "Space Shuttle Laminar Heating with Finite Rate Catalytic Recombination," AIAA Paper 81-1144, 1981.

3. Moss, J.N., Private Communication, 1982.

4. Fristrom, R.M. and McLean, W.J., 1982, "The determination of atom and radical concentration in flames using a scavenger microprobe." Presented at the Canadian Section of the Combustion Institute, Spring Meeting, May 1982.

Acknowledgments

The authors gratefully acknowledge the extensive advice and comments of a large number of researchers. Most of these scientists are currently engaged in related work and all provided valuable perspective for this study.

Princeton University:

G. Bienkowski
S.M. Bogdonoff
D. Dolling
I. Kennedy
M. Littman
G. Settles
A. Smits

NASA/Ames:

R. McKenzie

NASA/Langley:

D. Eide
J. Hoppe
W. Hunter
J. Junes
B. Lewis
J. Moss
J. Shinn
K. Sutton
G. Wood

United Technologies, Hartford, Connecticut:

M. Colket
A. Eckbreth
M. Sabielski
D. Seery

University of California, Berkeley, California:

J. Daily
L. Talbot

Sandia National Laboratory, Livermore, California:

R. Cattolica
R. Dibble
M. Dyer
W. Flower
D. Holve
W. McLean
L. Rahn
G. Ramback
R. Schefer
J. R. Smith
P. Witze

Stanford University, Stanford, California:

D. Baganoff
D. Bershader
R. Hansen
C. Kruger

APPENDIX A. RAYLEIGH SCATTERING

Rayleigh scattering is an elastic scattering process for which the scattering intensity is proportional to the number density of scattering molecules and therefore can be used to measure density. It is several orders of magnitude stronger than Raman scattering but lacks the species selectivity of Raman scattering and is easily obstructed by Mie scattering (in particle laden environments) and reflected laser light. It has been used for temperature measurements in constant pressure, non-reactive flows where the density and temperature are related through the equation of state [A.1]. The Doppler shift and broadening of the Rayleigh line can also be used to measure the velocity and temperature, respectively [A.2]. The Rayleigh scattering cross-section is species dependent, therefore a change in Rayleigh signal strength or line shape can be a result of composition changes as well as density or temperature changes.

The Rayleigh scattered signal strength, in terms of power, is given by the following expression:

$$P_{RAYLEIGH} = P_o \cdot L \Omega_C \eta_C \eta_D \sum_i N_i Q_i \qquad (A.1)$$

where P_o is the power of the incident laser beam, L is the length of the incident laser beam from which scattered light is collected, Ω_C is the solid angle of the collection optics, η_C is the efficiency of the collection optics, η_D is the detector quantum efficiency, N_i is the number density of species i and Q_i is the Rayleigh cross section for species i.

The sensitivity and accuracy of Rayleigh scattering for total density measurements was evaluated in terms of the minimum detectable density for a given signal to noise ratio. The noise was assumed to be quantum noise

which is equal to the square root of the number of detected Rayleigh photons. This leads to a signal to noise ratio:

$$(S/N)_{RAYLEIGH} = (P_{RAYLEIGH}\ \Delta t\ n_p/h\nu)^{1/2} \qquad (A.2)$$

where Δt is the pulse duration, n_p is the number of pulses during the measurement interval, h is Planck's constant and ν is the radiation frequency.

The experimental parameters used in equations (A.1) and (A.2) to determine the minimum detectable total density are those given in Table A.1 Two lasers were considered, a krypton fluoride (KrF) excimer laser and a copper vapor laser. The KrF because of its high average power and its UV output, which results in larger cross-sections and greater detector quantum efficiencies. The copper vapor because of its narrower output linewidth and higher efficiency. Based on the rate of descent of the Shuttle, an integration time of 10 seconds was chosen. The Rayleigh cross section for N_2 was used in this estimate, i.e. 8×10^{-28} cm^2/str-molecule at 514.5 nm. For a signal to noise ratio of 10, the resultant minimum detectable density is 3×10^{11}/cc with the KrF laser and 6×10^{12}/cc with the copper vapor laser. Both of these values are below the minimum density at the highest altitude. This result agrees well with a detection limit estimate made by Robert Dibble of Sandia-Livermore Laboratory who extrapolated from detection limits he routinely observes in the laboratory. He also estimated the error due to variations in composition to be less than ±15%. Therefore assuming we are in the quantum noise limit the use of Rayleigh scattering for total density measurements over the entire range of altitudes appears very promising. The problem of Mie scattering from particulates is an important concern since it will be orders of magnitude greater than the

Table A.1

Values Used for Rayleigh Scattering Signal to Noise Estimates

		KrF Laser	Copper Vapor Laser
Peak Power	P_o	40 MW	0.33 MW
Pulse Length	Δt	25 nsec	30 nsec
Repetition Rate	n_p	10^2/sec	5×10^4/sec
Wavelength	λ	249 nm	510 nm
Detector Quantum Efficiency	η_D	0.35	0.1
Collector Optics Efficiency	η_C	0.1	0.1
Optics Collection Angle	Ω_C	0.01 str	0.01 str
Scattering Length	L	5 mm	5 mm

Rayleigh scattering; however, if the particle density is not too high it is possible to identify and reject the larger signals due to particles [A.3].

To use Rayleigh scattering for temperature and velocity measurements, it is necessary to use a narrow line width laser (which rules out the use of the KrF laser) and a scanning Fabry-Perot spectrometer with adequate resolution, in order to resolve the Doppler shift and broadened line width which will both be of the order of 0.1 cm^{-1}. The number of detected photons will in turn be reduced, which will increase the minimum detection limit to approximately 10^{15}/cc. Since the minimum nitrogen density at 72 km altitude is also 10^{15}/cc, the Rayleigh temperature and velocity measurements will be possible at all altitudes, throughout the flow field. For the temperature measurement it will be necessary to correct for composition changes perhaps using the calculated Rayleigh lineshape [A.2], although the densities are so low that this latter effect is likely to be negligible.

References

A.1 Dyer, M.T., 1979, Rayleigh scattering measurements of time-resolved concentration in a turbulent propane jet. AIAA Journal 17, No. 8.

A.2 Cattolica, R., Robben, F. and Talbot, L., 1976, The interpretation of the spectral structure of Rayleigh scattered light from combustion gases. AIAA Paper No. 76-31.

A.3 Schefer, R.W., Dibble, R.W. and Driscoll, S.F., 1982, Mass fluxes $\overline{\rho'u'}$ and $\overline{\rho'v'}$ measured in a turbulent nonpremixed flame. Presented at 1982 Spring Meeting of the Western States Section of the Combustion Institute. Paper WSS/CI 82-35.

APPENDIX B. MIE SCATTERING

The presence of particles which have ablated from the space shuttle tiles are of interest for several reasons. One is that they represent a potential noise source for all of the optical diagnostics. Mie scattering, together with laser induced particulate incandescence and thermal emission could interfere with other optical measurements depending on the particle density and size distribution. It is essential to obtain information about the severity of these potential problems before implementing any of the optical techniques. This would require installing a window in the windward side of the re-entry vehicle. This window could be used to measure the intensity and spatial characteristics of the thermal emission from both the gas and the particles, as well as to look at the Mie scattering from a laser to get an estimate of the particle density, and, possibly, the size and spatial distribution.

The particles can also be used as a diagnostic seed for measuring velocity and temperature. Shortly after the particles are ablated from the tile surface they will be accelerated to the gas velocity. The time required to reach the gas velocity will depend on the particle mass and the gas velocity. The depth of penetration into the boundary layer will depend on the perpendicular momentum with which the particle was released from the surface. Within a certain distance from the surface there will be some particles which have not yet equilibrated with the gas velocity. It is necessary to determine which particle velocities correspond to the gas velocity. One approach is to simply take the velocity of the fastest particles to be that of the gas. Another method is to measure both the size and the velocity

simultaneously and to assume that the small particles are most likely to be travelling at the gas velocity. Such information could be obtained from a dual beam laser Doppler velocimetry system where the particle size is obtained from the visibility parameter of the Doppler burst. Unfortunately this method requires a priori knowledge of the particle size range since the visibility parameter is single valued over only a limited range of particle sizes. No other simultaneous velocity and particle sizing technique has been demonstrated to a reasonable degree of satisfaction. Dr. Donald Holve of Sandia-Livermore suggested using single beam methods, i.e. transit time velocimetry for velocity and pulse height detection for particle size, whereby velocity and size distributions could be obtained but not velocity-size correlations [B.1,B.2]. Techniques where one looks at the angular distribution of the Mie scattered light would be difficult to interpret because of the unknown and irregular particle shapes. Additional details on velocity measurement techniques can be found in the sections on laser Doppler velocimetry and resonant Doppler velocimetry. Another possibility for measuring the particle velocity which was suggested by Dr. Holve is to use double pulse or streak photography where, for example, a particle travelling at 1 km/sec would travel 1 mm during a 1 microsecond light pulse. Spatial resolution would be determined by the depth of field of the camera optics.

The particles could also be used to give an indication of the gas temperature by looking at the spectral distribution of the thermal emission from the particles. One would have to make some assumptions about the particle emissivity to determine its temperature and then the question of thermal equilibrium between the particle and the gas would still have to be

considered. As discussed in the section on Rayleigh scattering, a combined Mie scattering and Rayleigh scattering experiment looks promising as a method for determining particle densities.

References

B.1 Holve, D.J., 1980, In situ optical particle sizing technique. J. Energy 4, No. 4, pp. 176-183.

B.2 Holve, D.J., 1982, Transect timing velocimetry (TTV) for two-phase reacting flows. Combustion and Flame 48, No. 1.

APPENDIX C. LASER INDUCED FLUORESCENCE

Laser induced fluorescence has the potential of measuring rotational and vibrational temperature and species concentration and of performing density sensitive flow visualization. Generally one or more laser beams are directed into the flow to excite a particular species to a higher energy level. A detector then collects the fluorescence as the gas relaxes back to its initial state after a characteristic lifetime. The detector may be configured to monitor any position along the laser beam to give good spatial resolution. The fluorescence intensity is proportional to the population of absorbing molecules in the radiating upper energy level during the excitation process. This population is related to the total population through the rate equations which include the processes of spontaneous emission, stimulated emission, absorption, collision quenching, rotational redistribution, and vibrational redistribution. Unfortunately, the parameters describing these competing processes are not always known; particularly, the identity, concentration, and quenching rates of all possible collision partners are important and largely unknown quantities.

Temperature and species concentration measurements using laser induced fluorescence have been demonstrated at pressures equal to or less than one atmosphere and at temperatures up to those found in typical combustion environments (about 2000°K). The most frequently treated species has been OH, because of its important role in combustion kinetics; however, work has also been performed on numerous other systems including NO, N and O [C.1 - C.4] which are of interest in this study.

Several schemes have been proposed to account for the effect of quenching on the experimental results. One method, as first proposed by

Piepmeier [C.5], requires saturating the upper energy level and thereby eliminating the dependence on laser intensity as well as the need to correct for quenching. Since complete saturation is difficult to achieve, Baronovski and McDonald [C.6] proposed and demonstrated a partial saturation technique whereby one can extrapolate to the complete saturation limit. Another method, proposed and demonstrated by Stepowski and Cottereau [C.7] does not require saturation but requires that the laser pulse duration be shorter than the time for steady state conditions to be reached. The quenching rate then can be related to the fluorescence decay curve. The required laser pulse duration and the fluorescence decay rate will depend on the gas pressure and temperature. Other methods include the use of empirical quenching corrections as in the work of Muller et al. [C.8], and the use of detailed multi-level models as in the work of Chan and Daily [C.9] and that of Kotlar, Gelb and Crosley [C.10].

The most promising approach given the low density conditions is to determine the quenching rate from the fluorescence decay rate as has been done by Stepowski and Cottereau [C.7] for OH in a low pressure flame and by Bischel, Perry and Crosley [C.11] for both O and N atoms in a low pressure flow discharge. Based on the results of the latter work and the similarity between the excited electronic state lifetimes for OH and NO, a laser pulse width of less than 5 nsec is required. For O and N atom fluorescence, two-photon absorption is required because the first resonance transition lies far into the VUV. As Bischel et al [C.11] have demonstrated, one would detect the resultant near IR fluorescence. For NO the resonance transition can be accessed by either single or two-photon absorption. The disadvantage of the two photon process is that it is non-linear in laser

power. The advantage is that it is less difficult to generate tunable stable, high power visible radiation than the UV radiation required for the single photon process. There was no concensus among the researchers interviewed on this point. In either case the best laser system would be a Nd:YAG pumped dye laser using frequency doubling and/or Raman shifting to generate the required UV wavelengths.

After quenching has been accounted for, the fluorescence intensity gives the population of the lower energy level before laser excitation which can then be related to the total population if the temperature is known. The fluorescence technique can also be used to find the temperature by measuring the population of two or more energy levels since the ratio of the population of any two levels is equal to the ratio of the corresponding Boltzmann factors.

Of particular interest to this study is the work of McKenzie and Gross [C.2] who have demonstrated single pulse temperature measurements of NO seeded into a flow of nitrogen. A selected rotational level is two photon excited and its fluorescence monitored. A very short time thereafter a second laser pulse two photon excites the NO from a different rotational level to the same upper state. The ensuing fluorescence intensity due to each pulse can be related to the rotational populations in the two ground states, the ratio of which can be related to the rotational temperature. Since only the ratio of energies absorbed needs to be known, the redistribution of energy among rotational and vibrational levels of the excited state and their non-radiative quenching has a negligible effect on the measurement. This is true provided the quenching rate is insensitive to the rotational quantum number and broad-band detection is used. McKenzie considered the

transition $A^2\Sigma^+$, $v' = 0 \rightarrow X^2\Pi_{1/2}$, $v'' = 0$ in NO from the $J'' = 7\frac{1}{2}$ rotational level since it has the largest absorption coefficient at room temperature and is separated far enough from other lines to allow selective excitation. He obtained a signal to noise ratio (SNR) in the quantum noise limit of 200 for a single 1 millijoule pulse energy of 5 nsec duration. The NO concentration which he used was 2×10^{14} cm^{-3} at room temperature and the size of the probe volume was 0.1 mm x 1.0 mm. The maximum density of NO in the flow surrounding the re-entry vehicle is an order of magnitude higher at an altitude of 75 km. At this higher temperature the NO molecules distribute over more states thus lowering the density in any given vibrational rotational level. The signal is further reduced because of the increased quenching due to the higher temperature.

The minimum NO density downstream of the shock is 10^{14} cm^{-3} and the NO may have a translational temperature as high as 16,000°K. Scaling calculations were made for both 16,000°K and 3000°K and yielded a SNR of 9 and 40 respectively for a single 1 mJ pulse. The lower temperature was chosen due to the expectation that internal modes and chemical reactions will rapidly cool the translational energy of the gas, substantially lowering the rotational temperature. Increasing the laser's intensity to improve the SNR is limited by Stark broadening. The broadening reduces the laser energy coupling into the transition and may cause several lines to coalesce so that a particular rotational level may no longer be preferentially pumped. McKenzie has not yet quantified this limitation.

To determine the density detectability limit for a quantum noise limited signal to noise ratio of 10, a laser operating at 10 pulses per second with 1 mJ per pulse was considered. The integration time was assumed to be 10 seconds. The NO detectability is then found to be 1.5×10^{13} cm^{-3} and $7.5 \times$

10^{11} cm^{-3} for a temperature of 16×10^{3}°K and 3000°K respectively. The NO number density in most of the region between the shock and the vehicle surface at an altitude of 75 km is predicted to be between 10^{14} cm^{-3} to 10^{15} cm^{-3}. A comparison of Figures 4 and 5 in the main text of this report shows that the NO concentration drops quickly as the altitude decreases and by 47 km it is negligible except in the boundary layer. Consequently the laser induced fluorescence technique is only useful at the higher altitudes.

In summary measurements of NO, N and O concentrations and NO rotational temperature appear feasible at 75 km where appreciable concentrations are expected. Such measurements have been demonstrated under similar but not identical conditions. Thermal emission from the high temperature gas behind the shock and hot particles as well as Mie scattering from particles should be investigated as a potential problem. It would therefore be advisable to monitor the environmental conditions before a laser induced fluorescence measurement is carried out.

References

C.1 Bischel, W.K., Perry, B.E. and Crosley, D.R. Detection of fluorescence from O and N atoms induced by two-photon absorption. Applied Optics, Vol. 21, No. 8, April 1982.

C.2 McKenzie, R.L. and Gross, K.P. Two-photon excitation of nitric oxide fluorescence as a temperature indicator in unsteady gasdynamic processes. Applied Optics, Vol. 20, No. 12, June 1981.

C.3 Bradshaw, J. and Davis, D.D. Sequential two-photon-laser-induced fluorescence: a new method for detecting atmospheric trace levels of NO. Optics Letters, Vol. 7, No. 5, May 1982.

C.4 Bradshaw, J., Rodgers, M.O. and Davis, D.D. Single photon laser-induced fluorescence detection of NO and SO_2 for atmospheric conditions of composition and pressure. Applied Optics, Vol. 21, No. 14, July 1982.

C.5 Peipmeier, E.H. Theory of laser saturated atomic resonance fluorescence. Spectr. Acta., Vol. 27B, p. 431, 1972.

C.6 Baronovski, A.P. and McDonald, J.R. Measurement of C_2 concentrations in an oxygen-acetylene flame: an application of saturation spectroscopy. J. Chem. Phys., Vol. 66, No. 7, p. 3300, April 1977a.
Baronovski, A.P. and McDonald, J.R. Application of saturation spectroscopy to the measurement of C_2, $3\pi_u$ concentrations in oxy-acetylene flames. Appl. Opt., Vol. 16, No. 7, July 1977b.

C.7 Stepowski, D. and Cottereau, M.J. Direct measurement of OH local concentration in a flame from the fluorescence induced by a single laser pulse. Appl. Opt., Vol. 18, p. 354, 1979.

C.8 Muller, C.H., Schofield, K., Steinberg, J. and Brorda, H.P. Sulfur chemistry in flames. Seventeenth International Symposium on Combustion, 1978, p. 867.

C.9 Chan, C. and Daily, J.W. Measurement of OH quenching cross-sections in flames using laser induced fluorescence spectroscopy. Presented at the Western States Section of the Combustion Institute, Spring Meeting, Provo, Utah, Paper #79-20, 1979.

C.10 Kotlar, A.J., Gelb, A. and Crosley, D.R. A multilevel model of response to laser fluorescence excitation in OH. Presented at the ACS Symposium on Laser Probes for Combustion Chemistry, Washington, D.C., Sept. 1979.

C.11 Bischel, W.K., Perry, B.E. and Crosley, D.R. Detection of fluorescence from O and N atoms induced by two photon absorption. Appl. Opt., Vol. 21, p. 1419, 1982.

APPENDIX D. MASS SPECTROSCOPY

Mass spectroscopy can be used to separately measure the concentrations of O_2, N_2, NO, O and N over the entire range of densities that are expected during re-entry. In addition, using a mass spectrometer with a fixed collector plate detector, as has been proposed by George Wood of NASA Langley, would enable simultaneous measurements of all these species. A similar spectrometer has been built and successfully tested by Lehotsky [D.1]. Dr. Martin Zabielski of United Technologies pointed out that the sample flow rate between the altitudes of 80 and 40 km would change by approximately a factor of 10 for a fixed orifice area and given pumping system. He suggested that the pumping system be designed for 40 km and then simply overpumped at higher altitudes. This would permit continuous measurements to be made at all altitudes.

If effusive collection is used, (the collection orifice diameter less than the mean free path) then the sample would come from within a few mean free paths of the surface. This may cause difficulty since the gas composition within a few mean free paths of the collection orifice may be affected by the presence of the orifice which is likely to be made of a different material and at a different temperature than the surrounding tiles. Dr. David Seery of United Technologies suggested that it may be possible to use a larger orifice and collect the sample by modest pumping which, because of the low densities, would cause minimal distrubance to the flow field. By pumping on the orifice one would extend the sample volume further out into the flow field, beyond the region which is affected by the local surface reactions.

A major problem in using mass spectroscopy is the extraction of a sample which reflects the true composition of these gases. Radical species, particularly O and N atoms, quickly react or recombine. Because of the thckness of the tiles protecting the surface of the re-entry vehicle and the necessity to thermally insulate the mass spectrometer from the exterior temperatures, the sample must travel several inches before being analyzed. In order to minimize the effect on the local flow field, the passageway through the tiles should be small, e.g. a differential pumping, skimmer collection system could not be used. With the sample having to travel through a long, narrow passageway, both wall and gas phase collisions, and in turn O and N atom recombination reactions, will be inevitable. Wood has proposed selecting the wall material such that the O and N atoms selectively react upon collision with the wall producing a stable and identifiable species which would in effect serve to tag the original atomic species. Drs. Daniel Seery and Med Colket of United Technolcgies and Dr. Robert McLean of Sandia-Livermore, all suggested using the scavenging probe concept proposed by Fristrom and recently demonstrated by Fristrom and McLean [D.2]. Here, the sample is immediately diluted at the orifice with a gas stream containing a species which selectively reacts with either the O or N atoms to produce a stable and identifiable species. This species then serves to tag the original atomic species. If this stable product were already present in the sample then it might be possible to distinguish between the sample and the tag molecule by using different isotopes.

Another possibility suggested by Seery and Colket is to extend a traversing scavenging probe out into the boundary layer in order to extract samples at different distances from the wall. They felt that because of the

very high velocities that all appreciable disturbances to the flow field would be convected downstream and would not affect the measurement. They did point out, however, that when the flow is supersonic, as it is outside the subsonic boundary layer, there will be a shock in front of the probe which may substantially alter the sample's composition.

The general conclusion of this review is that using a scavenging probe to extract the sample with subsequent mass spectroscopic analysis is a promising technique for determining the concentrations of N_2, O_2, O and N near the wall and even possibly somewhat away from the wall into the boundary layer by using a traversing probe or by modest pumping rates.

References

D.1 Lehotsky, R.B., 1973, A mass spectrometer sensor system for metabolic analysis and atmospheric monitoring on Skylab and future manned spacecraft. Proceedings of the 21st Annual Conference on Mass Spectrometry and Allied Topics, May 20-25, 1973, San Francisco, CA, p. 403.

D.2 Fristrom, R.M. and McLean, W.J., 1982, The determination of atom and radical concentration in flames using a scavenger microprobe. Presented at the Canadian Section of the Combustion Institute, Spring Meeting, May 1982.

APPENDIX E. THERMAL EMISSION

Thermal emission from atoms and molecules may be used to measure temperature, identify species and perform density sensitive flow visualization. Thermal emission from hot particles may also be used to obtain the particle's temperature and velocity. It may alsc constitute a noise source for other optical nonintrusive techniques.

The fact that the collected signal is integrated over a path length prevents this technique from yielding good spatial resolution. Since most flows are inhomogeneous, an integration must be performed on the flow parameters as well. The problem is compounded if optically thin and optically thick regions are present along the path since the method for analysis of each of these regions is different. A major source of uncertainty in the optically thin limit is due to incomplete knowledge of quenching rates and Franck-Condon factors.

In a nonequilibrium gas, the concept of temperature is not defined. Usually the translational modes quickly equilibrate and thus most accurately reflect the temperature of the local environment. The translational temperature of an optically thin gas can be measured by resolving the spectral line profile of the emission from a particular transition. The profile has to be taken by using an interferometer to achieve high enough resolution. For a purely thermally broadened line, the frequency full width at half maximum, $\Delta\nu$, is related to the gas temperature, T, by [E.1],

$$T = \left(\frac{\Delta\nu\ \lambda_{21}}{2}\right)^2 \frac{M}{2k\ \ln 2} \qquad (E.1)$$

where λ_{21} and M are the emission wavelength and mass of the particular species and k is Boltzmann's constant. When using this relation to measure T

it is essential to account for the instrumental width and collision broadening.

The population of the various energy levels may reach separate thermodynamic equilibria which differ from the translational temperature and persist for a relatively long time. The temperature parameter in the Boltzmann distribution of energy level populations may be measured in a variety of ways. The emission intensity, I_{21}, from an optically thin source using the Boltzmann population factor is [E.2]

$$I_{21} = K\, g_2 \frac{A_{21}}{\lambda_{21}} \exp(-E_2/kT) \qquad (E.2)$$

where K is a constant, g_2 is the degeneracy of the excited level, A_{21} is the Einstein spontaneous emission coefficient of the transition, and E_2 is the energy of the excited state. Apart from uncertainties regarding the optical depth, the major errors involved in using this method are uncertainties in the Einstein A coefficients and quenching rates. Equation (E.2) may be applied to electronic, vibrational, or rotational population levels depending on the excitation energy.

Both the translation and the population temperature measurement techniques depend on the gas being optically thin. As the gas turns optically thicker, the emission spectrum approaches the black body curve as shown in Figure E.1. The black body temperature can then be determined from the peak intensity of an emission line. Since absolute intensity measurements are prone to error, fitting the black body curve to several separated peaks of optically thick lines is more accurate. The expression for the flux of radiation I_o per unit wavelength and unit solid angle is [E.1]

$$I_o = \frac{2hc^2}{\lambda^5} \frac{1}{e^{hc/kT\lambda} - 1} \qquad (E.3)$$

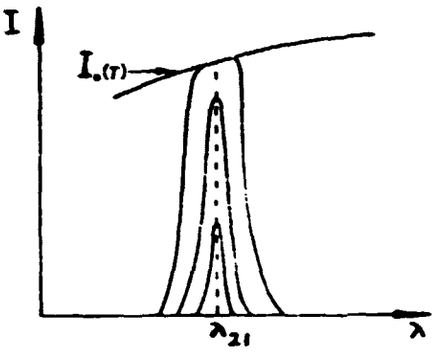

Figure E.1 An optically thick line approaches the black body radiation curve, $I_o(T)$.

where h is Planck's constant and c is the speed of light. The measurements should be performed near the peak of this curve where the sensitivity to temperature variation is largest so as to enhance the accuracy. Since at high temperature the peak is in the UV and at low temperature it is in the IR, it is not always possible to satisfy this condition with one spectrometer.

Thermal emission allows separate species to be observed since each atom or molecule has a characteristic spectrum. The species participating in the emission process may be identified by passing the collected light through a spectrometer. A measurement of the relative concentrations of these species is complicated by the different emission coefficients and optical quenching in the optically thin limit and different emissivities and optical depth in the optically thick limit.

The spectral profile of emissions from hot luminous particles may also be resolved by using a spectrometer. The temperature of these particles can be obtained by fitting the spectrum with the black body distribution given in equation (E.3). The particle's temperature may deviate from the gas temperature particularly in regions of high velocity and high temperature gradients in the flow.

A method has been developed to measure hot luminous particle velocities using a time of flight technique [E.3]. Two points of known separation in the flow are focused onto two different detectors. As the particle passes through, its emission is picked up by the detector as two pulses. One can determine the velocity by the difference in arrival time between the pulses. The spots have to be far enough apart to provide accurate time measurement but close enough to contain less than two particles. The vector connecting the two sample points in the flow has to be close to the particle trajectory

to ensure signal detectability. Problems similar to those associated with the classical laser Doppler velocimetry exist for this method, particularly, the inability of particles to follow the flow in regions of high accelerations.

The most serious aspect of thermal emission is its potential as a noise source which may obscure other measurements. An estimate of the noise intensity begins with the radiative transfer equation [E.4]

$$\frac{1}{c}\left(\frac{\partial I_\lambda}{\partial t}+\frac{c\partial I_\lambda}{\partial s}\right) = J_\lambda \left(1+\frac{\lambda^5}{2hc^2}\ I_\lambda\right) - K_\lambda\ I_\lambda \qquad \text{(E.4)}$$

where I_λ emission is the intensity, s is the displacement along a ray of light, and J_λ and K_λ are the emission and absorption coefficients per unit wavelength respectively. The emission and absorption coefficients may be related by invoking detailed balance. For the radiation to be in thermodynamic equilibrium, the medium has to be optically thick at all frequencies. Alternatively, one can assume that collisional processes are much more important than radiative. In other words, the excited state has a much higher probability of de-excitation by an inelastic collision than by spontaneous emission. A temperature may then be defined that fits the Boltzmann, Saha and Maxwell relations for the excited and ionic populations and velocity distributions. The radiative transfer equation at steady state may then be rewritten using Kirchhoff's law as [E.4]

$$\frac{\partial I_\lambda}{\partial s} = K'_\lambda(I_o - I_\lambda)\ . \qquad \text{(E.5)}$$

where I_o is the black body intensity distribution (E.3) and

$$K'_\lambda = K_\lambda(1 - e^{-hc/kT\lambda}) \qquad \text{(E.6)}$$

The equation may be integrated analytically for a homogeneous radiating plane layer of finite thickness, d [E.4].

$$I_\lambda(d) = I_o(1 - e^{-K'_\lambda d}) \tag{E.7}$$

A schematic of the detection configuration expected on a re-entry vehicle is shown in Figure E.2. The hot region between the shock and the wall is radiating. It is assumed for simplicity that the gas is homogeneous though very sharp gradients exist. This is justified by the fact that the high temperature regions dominate the radiation and will be used for estimating the emissions. A lens which is used to collect the signal generated by one of the nonintrusive optical techniques also collects background light due to thermal emissions. The thermal emissions are a distributed source so light is collected from regions other than the focal volume. It may be shown that the light is gathered from an equivalent truncated conical volume defined by the aperture and the lens as indicated in the figure. Equation (E.7) may then be integrated to yield

$$I_{\lambda a} = \frac{\pi}{4} I_o \tau(F)^{-2} \tag{E.8}$$

where F is the f number of the collection optics (F = lens focal length/lens diameter) and $\tau = K'_\lambda d$ is the optical depth (assumed to be $<<1$). The absorption coefficient per meter in hot air ($T < 20{,}000°K$) is taken from Zeldovitz and Raizer [E.4].

$$K_\lambda = 8.6 \cdot 10^{19}\, \rho \cdot T \cdot \lambda^3\, e^{\frac{1.44 \cdot 10^{-2}}{\lambda \cdot T}} \left(C_{O_2}\, e^{\frac{-140{,}000}{T}} + C_{N_2}\, e^{\frac{-181{,}000}{T}} + \right.$$

$$\left. C_O\, e^{\frac{-158{,}000}{T}} + C_N\, e^{\frac{-169{,}000}{T}} + C_{NO}\, e^{\frac{-108{,}000}{T}}\right) \tag{E.9}$$

where ρ is the density in Kgm/m^3, T is in °K, λ is in meters and C_i is the concentration of species i. K_λ and I_o have been plotted for different temperatures versus wavelength in Figures E.3 and E.4. The flow conditions

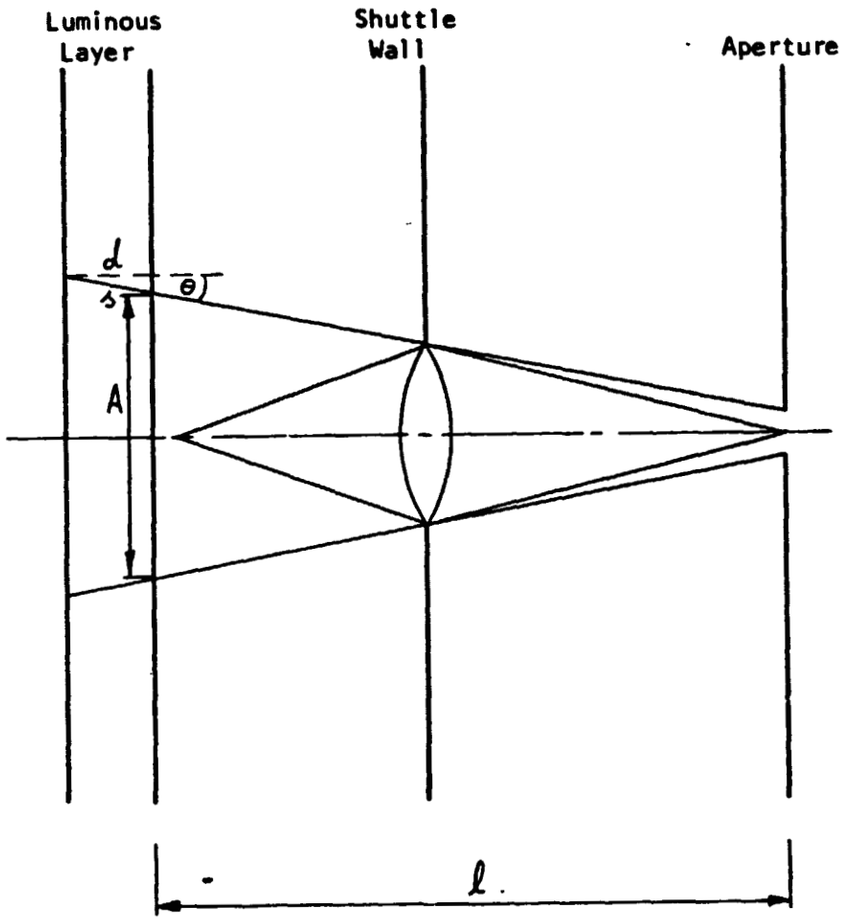

Figure E.2 Optical configuration showing location of shock, luminous layer, Space Shuttle wall with lens and aperture.

Figure E.3 Absorption coefficient (Equation E.10) versus wavelength for various temperatures. The flow conditions assumed are given by Moss's calculation for nonequilibrium flow, fully catalytic wall at an altitude of 75 km and $s/R_N = 10$.

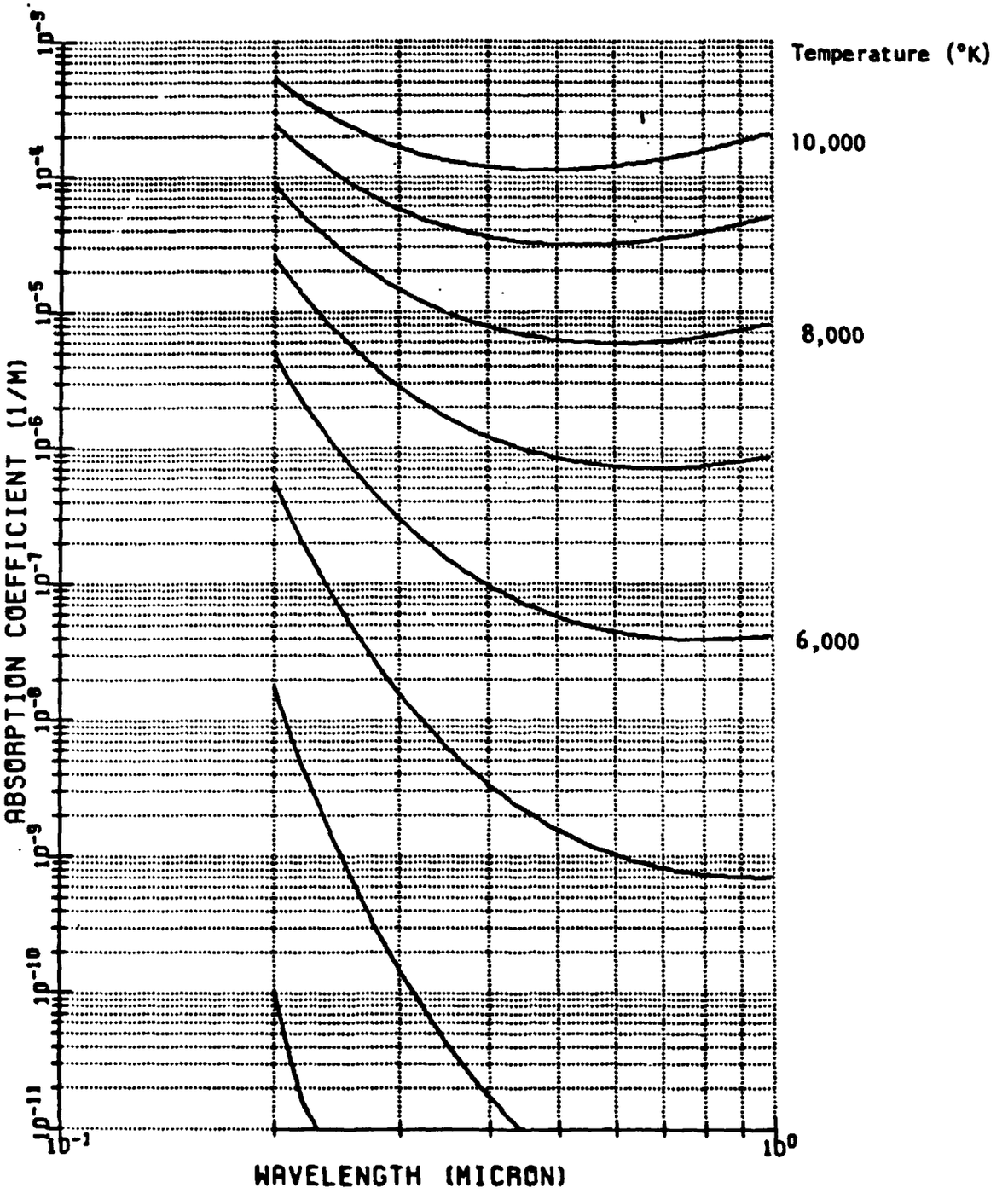

Figure E.4 Black body radiation versus wavelength at different temperatures.

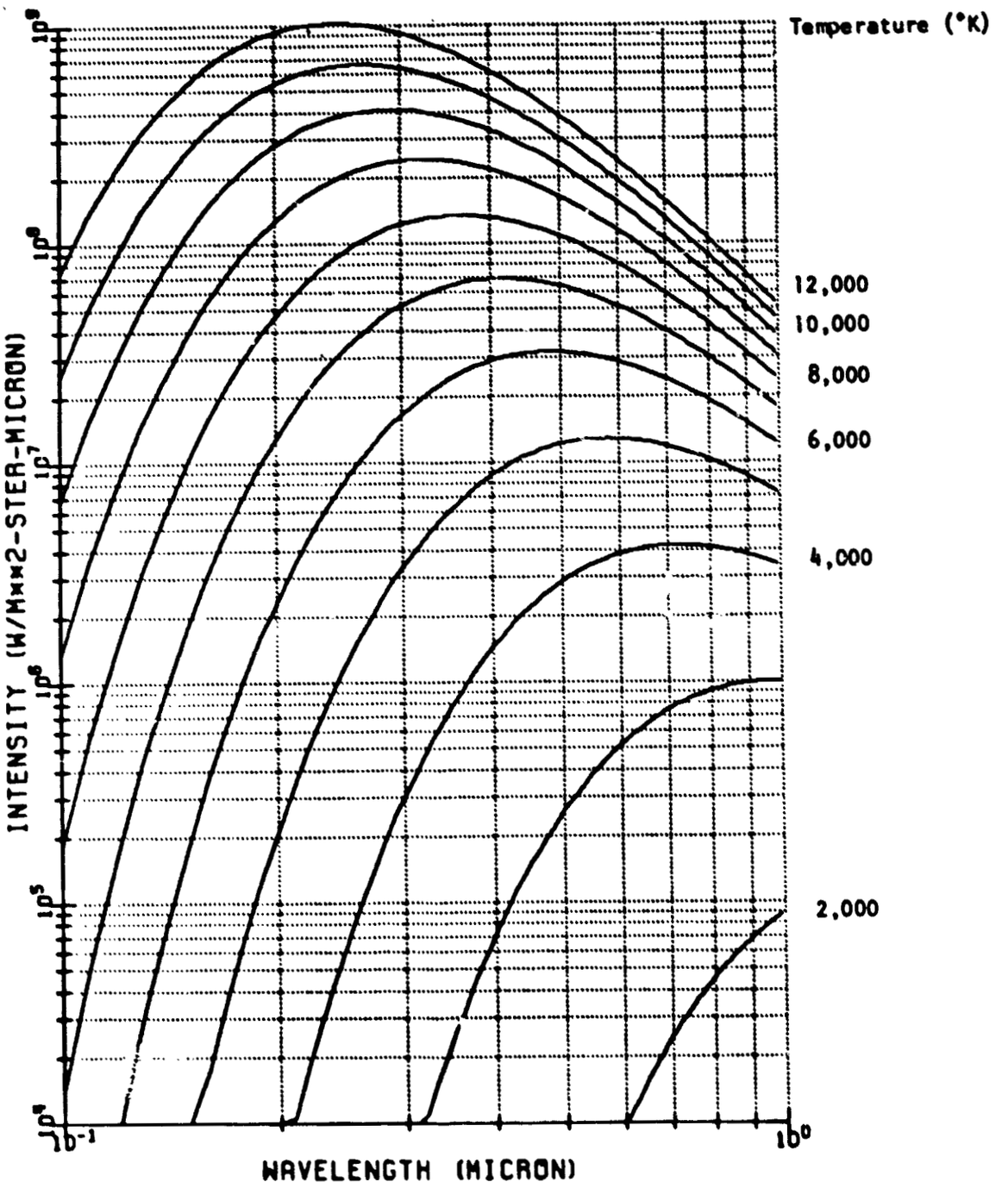

assumed are taken from the simulation by J.L. Shinn, J.W. Moss and A.L. Simmonds of NASA Langley for a nonequilibrium flow, fully catalytic wall calculation at an altitude of 75 km and at a position along the surface of the Shuttle corresponding to 10 nose radii.

As an example, consider:

$d = 0.1$ m

$\lambda = 510$ nm (copper vapor laser)

$F = 10$

$T = 10^4$°K

$\Delta\lambda = 0.1 \times 10^{-9}$ m (state-of-the-art interference filter)

From Figures E.3 and E.4, $I_o = 2 \times 10^8$ W/m$^2\mu$ and $K_\lambda = 1.1 \times 10^{-4}$ m^{-1}. The optical depth, τ, is $1.1 \times 10^{-5} << 1$ and equation (E.9) may be used. The intensity radiated into the aperture is 2×10^{-3} W/m^2. By comparison, the region in the flow at a temperature of 3000°K contributes only 10^{-15} W/m^2 and may clearly be neglected.

In summary, thermal emission from gases does not seem to be a promising method as far as quantitative measurements are concerned. This conclusion arises from the integrated path which makes point observation impossible and the uncertainty regarding the values of the quenching rates and Franck-Condon factors which are necessary for unequivocal data reduction. On the other hand, thermal emissions contain information which can be utilized for nonquantitative species identification.

Thermal emissions from gases and particles constitute a noise background source for other optical nonintrusive techniques. The first experiment to be undertaken should include a monitor for thermal emissions. In particular, an optical multichannel analyzer would be able to take a complete

spectrum in a much shorter time than a scanning spectrometer. The spectrum would be indicative of the species existing in the flow. Bursts due to hot particles passing through the probe volume can be gated out or directed into a different channel for additional processing.

References

E.1 A.P. Thorne, Spectrophysics (Chapman and Hall, London, 1974).

E.2 N.A. Generalov, Methods of Experimental Physics 18B, R.J. Emrich, editor (Academic Press, N.Y., 1981).

E.3 J.D. Trolinger and M.J. Houser, Flight Dynamics Laboratory Technical Report AFWAL-TR-81-3080, 1981.

E.4 Y.B. Zel'dovich and Y.P. Raizer, Physics of Shock Waves and High-Temperature Hydrodynamic Phenomena (Academic Press, New York and London, 1967).

APPENDIX F. ELECTRON BEAM FLUORESCENCE

The electron beam fluorescence technique is used to measure the static, vibrational. rotational and translational temperatures of low density gaseous flows as well as determine species concentration, measure velocity and perform flow visualization. Reviews of this technique have been written by E. P. Muntz [F.1] and this discussion draws heavily on these works.

A collimated beam of electrons of about 1 mm in diameter is directed into a flow, exciting the gas constituents into higher energy levels. The species decay after a characteristic lifetime emitting fluorescence. An optical detector may be configured to monitor any position along the beam to give a spatial resolution of $\sim$1 mm^3. The resulting spectrum is characteristic of the composition, temperature, density and velocity of the gas. The many different parameters on which the electron beam fluorescence is dependent make it an attractive technique. Its use is usually limited to number densities of less than 10^{16} cm^{-3} though some investigators have extended the range to 10^{18} cm^{-3} [F.2]. The electron beam loses its collimation and penetration depth at higher densities and the fluorescence is no longer linearly related to density. Ambient temperatures and less have been measured and some work at up to 1000°K has also been performed [F.3]. The velocity sensitive feature of the electron beam fluorescence technique has been applied only in a few cases and then only to hypersonic facilities (1000 to 2000 m/sec) [F.4].

Nitrogen and air flows have been the most extensively investigated. The major emission in both occurs for the first negative system of N_2^+ at 391.4 nm. A 50,000 electron volt beam exciting the first negative system

of nitrogen with a 1 mA/mm^2 of current will produce 10^{11} photons per second. Incomplete knowledge with regard to quenching rates and Franck-Condon factors is the main limiting factor as far as data interpretation is concerned.

The most straightforward quantitative measurement is the nitrogen density. This requires a density independent transfer of energy from the electrons to the nitrogen excited state. There are several mechanisms for accomplishing this transfer: 1) Collision of nitrogen with primary high energy electrons originating from the electron beam; 2) Collision of nitrogen with secondary electrons produced by species ionization due to collisions with primary electrons; 3) Absorption of electron beam generated photons by unexcited nitrogen molecules; 4) Energy transfer by collisions of nitrogen with other excited particles; 5) Transfer of population to the excited state by cascade from higher electronic states. The excited state is subsequently depopulated by spontaneous emission and quenching collisions. The emission is observed as signal; the quenching collisions compete with emission and reduce the signal.

If only the primary electrons are assumed to populate the excited state then the fluorescence emission, I_{ik}, is related to the gas density, n_g, by [F.1]

$$I_{ik} = K n_g \frac{1}{1 + 2n_g \frac{Q_{gg} \bar{V}_{gg}}{A_{ik} + A_T}} \qquad (F.1)$$

where K is a constant, Q_{gg} is the quenching collision cross section, A_{ik} is the spontaneous emission for the transition of interest, A_T is the spontaneous emission for all other transitions and $\bar{V}_{gg}$ is the relative velocity between the molecules.

The plot of this relationship is shown in Figure F.1. At low density the emission, I_{ik}, is essentially proportional to the gas density. At

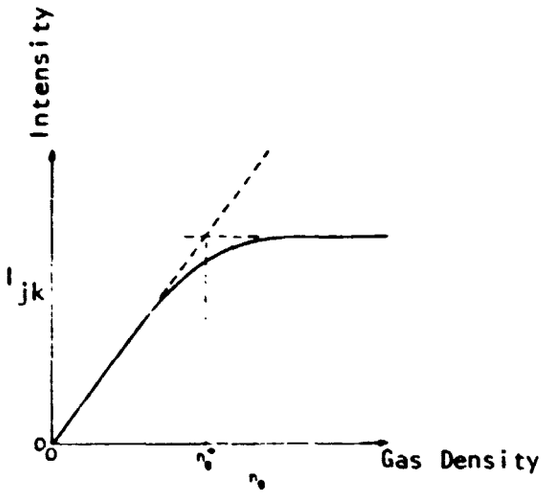

Figure F.1 The Electron Beam Fluorescence intensity saturates at densities above 10^{16} cm^{-3}.

higher densities the fluorescence intensity is strongly quenched and is no longer sensitive to density variations. Most density measurements are performed in the linear portion of the response curve. The accuracy of density measurement can approach ±1 percent if the calibration procedure is carefully executed; however, ±5 percent is more typical. The large number of scattered photons reduces photon statistical noise to a low level. Inaccuracies are introduced by the quenching process which is both species and temperature dependent.

Some experimental work has been carried out at higher densities [F.2] ($10^{16} \leq n \leq 10^{18}$ cm^{-3}). This is the nonlinear regime and a careful calibration is required over the complete range of density and temperature.

In a nonequilibrium gas, the vibrational and rotational energy level populations may not be in equilibrium with each other or with the local temperature. For example, the vibrational levels may separately reach an equilibrium which may be described as a temperature but is different from the true translational temperature of the gas. To measure this vibrational temperature, first consider a ground state molecule with vibrational level v_1'' excited to the v' vibrational state of the upper electronic level with subsequent decay to the v_2'' vibrational level of the ground electronic state. If only spontaneous emission depopulates the upper state and quenching is neglected, then the intensity of fluorescence is [F.1]

$$I_{v'v_2''} = K \nu^4_{v'v_2''} \frac{q(v',v_2'') \sum_{v_1''} n_{v_1''} q(v'v_1'')}{\sum_{v_2''} \nu^3_{v'v_2''} q(v'v_2'')} \qquad (F.2)$$

where K is a constant, ν is the frequency, n is the number density, and q is the Franck-Condon factor. The vibrational temperature information is

contained explicitly in the number density, $n_{v''_1}$, which is assumed to follow a Boltzmann distribution. By monitoring the fluorescence intensity from two separable vibrational lines and taking their ratio, one may obtain a curve which is temperature sensitive and independent of the constant K.

The technique has been checked at low densities and up to 300°K with a resulting accuracy of ±10% [F.5]. Quenching invalidates equation F.2 at higher densities. The number of vibrational levels involved in the calculation rises with temperature. This introduces an additional uncertainty due to the larger number of Franck Condon factors involved. Higher temperatures also have a bearing on the quenching process.

Similarly the rotational modes may reach a separate "temperature". The expression which provides the rotational temperature is rather involved, requiring an iteration process and will therefore not be given here. Similar difficulties to those associated with the vibrational temperature measurement are encountered with the rotational temperature measurement and they are related to uncertainties in the knowledge of quenching rates and Franck-Condon factors. The rotational temperature can in many cases be assumed equal to the translational temperature; however this is not always true for the vibrational temperature.

Low density is still a requirement to minimize quenching, but accuracies of better than ±5°K have been achieved at temperatures below 1000°K [F.6]. Large discrepancies exist for temperatures below 300°K. Their origin is still unknown.

The translational temperature is considered to be the true local temperature. The translational temperature may be obtained by spectrally resolving the fluorescence emission of a particular transition. The

instrument most frequently used is a Fabry-Perot interfereometer. The lineshape observed has a Gaussian component which is related to Doppler broadening due to the random motions of the molecules. The temperature of the flow, T, is related to the full width at half maximum, $\Delta\nu_G$, of the Gaussian lineshape by [F.1]

$$T = \left(\frac{\Delta\nu_G \cdot \lambda}{2}\right)^2 \frac{m}{2k \ln 2} \qquad (F.3)$$

where λ is the wavelength of the transition, m is the mass of a single atom and k is Boltzmann's constant. Under optimum conditions the technique can measure the translational temperature in helium with an accuracy of a few degrees K at room temperature. The accuracy in other gases depends on the fluorescence intensity and the ratio between the Doppler width and the collisional and instrumental widths.

Electron beam fluorescence can be used for velocity measurements by observing the Doppler shift of the fluorescence. A comparison of the fluorescence spectrum of a stationary gas with the same transition in moving gas gives the Doppler shift, $\delta\nu_D$. The velocity, U, may then be calculated from [F.4]

$$U = \delta\nu_D \cdot \lambda \qquad (F.4)$$

where λ is the wavelength of the observed transition. The relative accuracy of the measurement depends on the relative size of the Doppler shift, $\delta\nu_D$, in comparison to the combined temperature collisional and instrumental broadening, $\Delta\nu$. A tracking Fabry-Perot simplifies velocity measurements since it eliminates the need to scan the complete spectrum.

The fluorescence emission also provides a method for density sensitive flow visualization. Fluorescence in the close proximity to the electron

beam is observed for N_2, O_2 and NO. An afterglow is obtained in He flows due to the excitation of a metastable state. Hence while the gas fluoresces a long way downstream in He flows, in air the electron beam has to pass through the position of interest.

The researchers contacted all agreed that the utility of the electron beam technique is limited by insufficient knowledge of quenching rates which leads to large uncertainties in temperature measurements. It was felt by Professor Larry Talbot of the University of California-Berkeley and Dr. William Hunter of NASA Langley that electron beam fluorescence was most useful as a flow visualization tool. Dr. Robert Cattolica of Sandia-Livermore felt that it would be worthwhile to undertake measurements at very high altitudes. At high altitudes (somewhat above those of interest in this study) the densities will be low enough so that the data could be interpreted quantitatively. At lower altitudes quenching will eliminate this possibility, but gross features of the flow may still be observable.

In summary, the electron beam fluorescence technique is attractive due to the many properties which it can measure and the fact that the signal is not photon statistics noise limited. For linear operation, it can only be used at the highest altitude of interest. At lower altitude one could possibly apply it to density measurements only after careful calibration.

Major uncertainties in temperature measurements arise from insufficient knowledge of the quenching and Franck-Condon factors particularly at the high temperatures existing in the flow. Velocity measurements are best performed on atoms but have not been demonstrated on nitrogen or other species present in the flow. Since a fluorescence signal will also be present, it might be useful to use an electron beam at least for flow visualization

and try to extract quantitative data by proper calibration at the higher altitudes.

References

F.1 E.P. Muntz, Methods of Experimental Physics, 18B. R.J. Emrich editor, (Academic Press, New York, 1981).
E.P. Muntz, AGARDograph 132 (1969).

F.2 J.A. Smith and J.F. Driscoll, AGARD Conference Proceedings No. 193 on Applications of Non-Intrusive Instrumentation in Fluid Flow Research, AGARD CP-193 (Harford House, London, 1976), paper 16-1.

F.3 W.W. Hunter, AIAA J. 8, 959 (1970).

F.4 V. Natiello, Thesis, Princeton University, 1970 (unpublished).
M. Becker, F. Robben and R. Cattolica, AIAA J. 12, 1247 (1974).

F.5 G.O. Langstroth, Proc. Roy. Soc. A146, 166 (1934).
C.Y. Fan, Phys. Rev. 103, 1740 (1956).
J.R. Sheridan and K.C. Clark, Phys. Rev. 140, 1033 (1965).

F.6 D. Coe, F. Robben and L. Talbot, in "Rarified Gas Dynamics", R. Campargue editor, Abst. 160.C.E.A., Paris, 1978.
N.V. Karelov, A.K. Rebrov and R.G. Sharafutdinov, in "Rarified Gas Dynamics", R. Campargue editor, Abst. 135.C.E.A., Paris, 1978.

APPENDIX G. RAMAN SCATTERING

Raman scattering is an inelastic scattering process where the wave number shift of the scattered light is characteristic of the spacing between the scattering molecule's rotational, vibrational and/or electronic energy levels. Raman scattering can be used to measure the number density of the scattering species and the gas temperature.

For a specific rotational, vibrational and/or electronic energy level transition, A→B, the Raman scattered signal strength, in terms of power, is given by the following expression

$$P_R = P_o N_A \left(\frac{d\sigma}{d\Omega}\right)_R L \Omega_c \eta_c \eta_D \qquad (G.1)$$

where P_o is the power of the incident laser beam, N_A is the number density of the scattering species in energy level A, $\left(\frac{d\sigma}{d\Omega}\right)_R$ is the differential Raman scattering cross-section, L is the length of the incident beam from which scattered light is collected, Ω_c is the solid angle of the collection optics, η_c is the efficiency of the collection optics and η_D is the detector quantum efficiency.

The Raman scattered light corresponding to different energy level transitions therefore is at different wavelengths and its intensity is proportional to the population of the initial energy level. This results in a spectral shape which is a function of the relative energy level populations and which under equilibrium conditions can be related to the gas temperature. The integrated spectrum in turn is proportional to the total number density of the scattering species.

The sensitivity and accuracy of Raman scattering for species density measurements was evaluated in terms of the minimum detectable species

density for a given signal to noise ratio. The noise was assumed to be quantum noise which is equal to the square root of the number of detected Raman photons, therefore the signal to noise ratio is given by:

$$(S/N)_R = (P_R \Delta t \, n_p/h\nu)^{1/2} \qquad (G.2)$$

where Δt is the pulse duration, n_p is the number of pulses during the measurement interval, h is Planck's constant and ν is the radiation frequency.

In order to determine the minimum detectable number density for a given signal to noise ratio, the experimental parameters in equations (G.1) and (G.2) must be specified. The experimental parameters have been selected to give maximum signal strength and to be consistent with any constraints imposed by the proposed flow field measurements. The experimental parameters are summarized in Table G.1. Two lasers were considered, a KrF laser and a copper vapor laser. The KrF because of its high average power (1 J/pulse at 10 Hz) and its UV output (249 nm) which results in larger Raman cross-section and in greater detector quantum efficiencies. The copper vapor because of its high average power (10 mJ/pulse at 5000 Hz). The measurement length L is chosen to be 5 mm based on the spatial resolution required to characterize the boundary layer profiles which were predicted by the numerical computations. It is assumed that for the density measurements the integrated Raman spectrum would be used, in which case N_A becomes the total number density of the scattering species. Based on the rate of descent of the Space Shuttle, it is assumed that an integration time of 10 seconds could be used to make the measurements. In Table G.2 are listed the five species which are expected in the boundary layer, the Raman transition, the Raman cross-section and the minimum detectable density for a signal to noise ratio of 10. Results for both the KrF and the copper vapor laser are given.

Table G.1

Values Used for Raman Scattering Signal to Noise Estimates.

		KrF Laser	Copper Vapor Laser
Peak Power	P_o	40 MW	0.33 MW
Pulse Length	Δt	25 nsec	30 nsec
Repetition Rate	n_p	10^2/sec	5×10^4/sec
Wavelength	λ	249 nm	510 nm
Detector Quantum Efficiency	η_D	0.35	0.1
Collector Optics Efficiency	η_C	0.1	0.1
Optics Collection Angle	Ω_C	0.01 str	0.01 str
Scattering Length	L	5 mm	5 mm

Table G.2

Minimum Detectable Density by Raman Scattering Compared with Expected Maximum Densities at 75 and and 52 km Altitudes.

Species	Raman Transition	$\frac{d\sigma}{d\Omega}/\frac{d\sigma}{d\Omega}\Big\|^{*}_{N_2}$	Minimum Detectable Density with S/N = 10		Maximum Density	
			KrF	Copper Vapor	75 km	52 km
N_2	Vibrational 2332 cm^{-1}	1.0	4×10^{14}/cc	1.6×10^{16}/cc	3×10^{16}/cc	1×10^{17}/cc
O_2	Vibrational 1557 cm^{-1}	1.2	3.4×10^{14}/cc	1.3×10^{16}/cc	6×10^{15}/cc	2×10^{16}/cc
NO	Vibrational 1877 cm^{-1}	0.55	7.2×10^{14}/cc	2.8×10^{16}/cc	3×10^{15}/cc	1×10^{16}/cc
N	Not Applicable	---	----	----	----	----
O	Electronic 158 cm^{-1}, 226 cm^{-1}	1.26	3.2×10^{14}	1.3×10^{16}	6×10^{15}/cc	2×10^{16}/cc

* $\frac{d\sigma}{d\Omega}\Big|_{N_2} = 4.4 \times 10^{-31}$ cm^2/str-molecule with 5145Å laser.

The detectability estimates given in Table G.2 can be compared to the calculated species densities at different altitudes, which are also summarized in Table G.2, in order to determine the altitudes at which Raman scattering concentration measurements are possible. Based on these results and the requirement of a dynamic range of 10, it can be concluded that with the KrF laser N_2, O_2, NO and O can be measured at all altitudes; whereas with the copper vapor laser, N_2 can be measured at altitudes up to 60 km while O_2, NO and O can be measured at altitudes up to 52 km. It is important to re-emphasize that these detection estimates are made assuming no appreciable background noise due to particulates (i.e. scattering or incandescence) or thermal emission.

The calculations predict that the nitrogen mass fraction varies by less than 30% across the boundary layer profile for a given altitude and distance along the vehicle, therefore from the point of view of characterizing the reacting nature of the boundary layer flow, the nitrogen density is of little interest. However, the gas density does change by approximately a factor of 10 over a given boundary layer profile, therefore a nitrogen density measurement could be used as a measure of the total gas density.

For temperature measurements one should use the most populous species, if possible, which in this case would be nitrogen. As shown above, using a KrF laser the detection of total N_2 concentration is possible at all altitudes. However, if one chooses to resolve the Q-branch spectrum for the purpose of curve fitting to determine the temperature, the partitioning of the signal among the different vibrational-rotational levels will increase the minimum N_2 density at which thermometry measurements can be made by a factor of 100. In this case thermometry measurements would only be possible

at 52 km and below. If a vibrational band ratio or Stokes/anti-Stokes approach is used for larger signal strengths, then the partition factor is in the worst case 10 and thermometry measurements can be made at all altitudes.

Assuming temperature measurements could be made from the nitrogen vibrational Raman spectrum as discussed above, one would have to be concerned, especially near the shock, about non-equilibrium effects, i.e. whether the measured vibrational temperature was in equilibrium with the gas kinetic temperature.

Another possibility for enhanced signal strengths would be to use resonance Raman scattering off of O_2 (193 nm) or NO (220 nm) whereby several orders of magnitude greater signal strengths could be realized. As pointed out by Dr. Alan Eckbreth of United Technologies, this would require the use of a laser with excellent frequency stability. There are, however, no reports in the literature of reonsnace Raman measurements of O_2 or NO therefore little more can be concluded at this time.

The concensus of the researchers we interviewed was generally not as optimistic as these results, however most of their concerns were related to the potential problem of background noise from particulates and thermal emission. There was agreement that characterization of these potential noise sources must be done before the final experiment selection and design is completed. Because of the weak signals associated with spontaneous Raman scattering, there was also agreement that fluorescence and Rayleigh measurements should be given serious consideration.

APPENDIX H. COHERENT ANTI-STOKES RAMAN SCATTERING

Coherent anti-Stokes Raman scattering (CARS) is a three photon, inelastic scattering process which is enhanced as the difference in frequency between two incident laser beams nears resonance with an energy level transition of the scattering molecule. The scattered radiation is then at the Raman anti-Stokes wavelength. The intensity of the CARS signal, I_{AS}, at frequency ω_{AS} is given by the following equation.

$$I_{as} = \left(\frac{4\pi^2 \omega_{AS}}{c}\right)^2 I_p^2 I_S |\chi|^2 Z^2 \eta \qquad (H.1)$$

where

$$\omega_{AS} = 2\omega_p - \omega_S ,$$

$$\chi = \chi_R + \chi_{NR}$$

and

$$\chi_R = \frac{2Nc^4}{\hbar \omega_S^2} \left(\frac{d\sigma}{d\Omega}\right)_R \frac{\Delta\omega \, \Delta_J}{\Delta\omega - (\omega_p - \omega_S)^2 - i\gamma(\omega_p - \omega_S)} = \chi_R' + i\chi_R''$$

I_p is the intensity of the probe beam at frequency ω_p, I_S is the intensity of the Stokes beam at frequency ω_s, χ is the third-order nonlinear susceptibility, Z is the distance over which the beams interact, c is the speed of light and η is the combined interaction-collection-detection efficiency. The third-order susceptibility is composed of a resonant part χ_R and a nonresonant part χ_{NR}. The resonant part of the third order susceptibility is dependent on N, the total species number density, $\left(\frac{d\sigma}{d\Omega}\right)_R$ the Raman cross-section for the transition characterized by the frequency difference $\Delta\omega$, γ, the Raman line width, Δ_J, the fractional population difference between the levels in the transition and $\hbar$ is Planck's constant divided by 2π.

The CARS process is nonlinear in incident beam intensity, number density, and interaction length whereas spontaneous Raman scattering is linear

in these parameters. Because of this nonlinear behavior, for a given experimental situation, the CARS signal strength can be larger or smaller than the corresponding spontaneous Raman signal depending on the number density. The CARS process must also satisfy a phase matching requirement (i.e. conservation of momentum). Phase matching is possible with one-sided optical access, however a wide angle crossed beam configuration must be used. This results in a shortened interaction length and limited traversing capability.

In order to estimate the CARS signal strength, one can assume that the Stokes and anti-Stokes beams have the same diameter. Equation (H.1) can then be written in terms of the CARS power

$$P_{AS} = \left(\frac{4\pi^2 \omega_{AS}}{c^2}\right)^2 |\chi|^2 I_p^2 P_S Z^2 \eta \qquad (H.2)$$

There are two limiting cases to consider when estimating the minimum detection limits. One case is the detection of a major species for which $\chi_R > \chi_{NR}$, and the other is the detection of a minor species for which $\chi_R < \chi_{NR}$. We will consider the measurements to be quantum noise limited in both cases. In the former case the greatest source of noise is the quantum noise in the signal itself, therefore

$$(S/N)_{CARS} = \left(\frac{P_{AS}\, \Delta t\, n_p}{h\nu}\right)^{1/2} \qquad (H.3)$$

where $$|\chi|^2 = \chi_R'^2 + \chi_R''^2$$

In the latter case the major noise source is the quantum noise in the nonresonant background. Therefore the signal is the contribution due to $2\chi_R'\chi_{NR}$ and the noise is the square root of the contribution due to χ_{NR}^2. The ratio of these two reduces to equation (H.3) where $|\chi|^2 = 4\chi_R'^2$ is used in equation (H.2). Therefore the difference in the detection limit for the

major species and the minor species cases differs only by approximately a factor of two.

The minimum detectable nitrogen density for a signal to noise ratio of 10 can now be determined using equations (H.2) and (H.3). The assumed experimental parameters are listed in Table H.1. The resultant detectability limit is $10^{15}/cm^3$. This estimate is for 1500°K, however away from the surface the temperatures are expected to be much higher. As the temperature increases, the rotational population spreads out over many more levels which causes a reduction in the CARS strength through the Δ_J term in the third order susceptibility. And as Eckbreth pointed out, the contribution of adjacent lines will also be less at high temperature which will further reduce the CARS strength.

If we compare this result to the calculated densities of N_2, O_2, NO and O at different altitudes we conclude that N_2 can be detected at all altitudes and that O_2, NO and O can be detected at 52 km and below. Again, the sensitivity will be less in the hotter regions away from the surface. In order to relate the CARS signal strength to the density, it is necessary to know the gas temperature, unless a particular transition can be selected for which the population difference term is temperature independent. Determination of the temperature from the N_2 CARS spectrum requires resolving the spectrum which increases the minimum detection limits to $10^{17}/cm^3$ because of reduced χ_R away from the peak and the necessity to use broad band CARS. Thermometry measurements therefore will only be possible at the lowest altitude.

Because the detection limit analysis predicts adequate sensitivity at only the lowest altitudes and because of the severe limitation due to one side optical access, it is concluded that CARS is not viable for the proposed

re-entry vehicle measurement. Several of the researchers interviewed have had extensive experience using CARS diagnostics and their comments were in general agreement with this conclusion.

Table H.1
Values Used for CARS Signal to Noise Estimates.

First laser wavelength	λ_p = 532 nm
Second laser wavelength	λ_s = 607 nm
Observed wavelength	λ_{AS} = 480 nm
First laser peak power	P_p = 10 MW
Second laser peak power	P_s = 1 MW
Nonlinear susceptibility	$\chi_R = 3.2 \times 10^{-17}$ cm^3/erg at 1 atm, 1500°K
Combined efficiency	η = 0.01
Beam diameter	D = 200 μm
Pulse duration	Δt = 10 nsec
Total number of pulses integrated	n_p = 100
Interaction length	z = 200 μm

APPENDIX I. LASER DOPPLER VELOCIMETER

The laser Doppler velocimeter is useful for measuring fluid velocities. Laser light scattered by a particle moving with the flow experiences a Doppler frequency shift proportional to the velocity of the particle. A measurement of the shift in frequency then gives the particle velocity. The most commonly employed configuration uses two laser beams crossed in the sample region to produce interference fringes (Figure I.1). As the particle traverses this region it crosses the fringes (Figure I.2) at a rate determined by the velocity, resulting in scattered light which is modulated at the crossing frequency. Spatial resolution is defined by either the beam crossing volume or the collection optics with submillimeter resolution easily obtainable. A second approach employing a Fabry-Perot interferometer may be useful at high fluid velocities. The laser Doppler velocimeter is nonintrusive and insensitive to other fluctuating flow parameters such as density and temperature. Velocity ranges from 10^{-3} cm/sec to 10^{6} m/sec have been measured. The difficulties associated with the use of the laser Doppler velocimeter are primarily due to the fact that the flow has to be seeded and that the particles do not track the flow in regions of high acceleration or low density.

The detected signal arising from light scattered by the particles as they move through the set of interference fringes may be found from equation I.1 [I.1]

$$\frac{U_1}{\nu_B} = x_f = \frac{\lambda_o}{2 \sin \alpha/2} \tag{I.1}$$

Here U_1 is the particle velocity in the plane of the two laser beams and perpendicular to their bisector, α is the intersection angle, λ_o is the

laser wavelength, and ν_B is the beat frequency produced. The distance between the fringes is x_f. The product of the output of the frequency counter, ν_B, and the fringe spacing, x_f, equals the velocity. It is clear that for a given laser frequency and beam intersecting angle, the beat frequency is directly proportional to velocity. Commercial laser Doppler velocimeter units can handle counting rates up to 200 MHz. State-of-the-art counters can go as high a 1 GHz which is also approximately the largest bandwidth of available photomultipliers. Counter availability is therefore the limiting factor as far as high velocity measurements are concerned. Table I.1 lists the counting frequencies, ν_B, for different beam intersecting angles, α, for an argon laser operating on the $\lambda_o = 514.5$ nm line and a particle velocity of $U_1 = 5000$ m/sec.

Table I.1

Fringe Spacing and Counting Frequencies for .5145μ Laser Beams Intersecting at Angle α and 5000 m/sec Particles.

$\alpha°$	x_f (μm)	ν_B (MHz)
45	0.7	7000
20	1.5	3333
5	6	835
1	30	166

From the table it is clear that the smaller the angle the more manageable the counting rate. If this method is to be used with a re-entry vehicle, very small angles will be required. An alternative approach to reduce the counting rate is to shift the frequency of one of the laser beams so the fringes scan in the direction of motion. This eliminates part of the Doppler shift and is useful only if a narrow range of velocities are to be measured. A large value of interaction length permits one to focus several detectors at different positions along the interacting volume so as to obtain a velocity profile. Clearly the shallower the angle α the longer the interaction length becomes.

The second approach circumvents the high counting rate problem by resolving the scattered light spectrally. A Fabry-Perot etalon is inserted between the intersecting volume and the detector. Two peaks are registered by the detector as the etalon is scanned as shown in Figure 1.3. They correspond to the Doppler downshifted and upshifted light scattered by the two laser beams off the moving particles. The frequency difference between the two peaks is ν_B in equation (1.1). $\Delta\nu_o$ is the free spectral range of the Fabry-Perot which provides a frequency calibration. While an upper bound limits the velocity measureable with the optical mixing configuration, a lower bound exists if the scattered light is to be spectrally resolved. When both scattered signals are put through the same etalon the minimum measured velocity is limited by the Rayleigh criterion: a shift is measureable only if it is larger than the width of the spectral line, $\Delta v \leq \nu_B$, otherwise the two peaks coalesce. To overcome the limitation, a reference beam configuration may be employed whereby just one beam interrogates the flow while the other beam is used as a frequency reference. The scattered light from the flow and the reference beam are now directed into different etalons so that the peaks cannot overlap at small velocities. A single etalon may be employed if the frequency of the reference beam is shifted using a Bragg cell.

Two additional techniques which have been used and are related to laser Doppler velocimetry should be mentioned. One is the time of flight velocimeter [1.2] which may be used if the flow direction is known. Two parallel laser beams are directed into the flow. A detector monitors the light pulses scattered off the particles as they pass through the beams. The velocity is deduced from the known separation of the beams and the time difference between the light pulses.

In a related technique discussed by Dr. Don Holve of Sandia Laboratories the pulse shape of a particle traversing a single laser beam is resolved temporally and is independent of the particle size or trajectory. The time between two fractional values of the peak amplitude is related to the particle's velocity. The intensity of the pulses can also be used to obtain the particle size distribution, however velocity-size correlations cannot be determined [I.3].

Two extensions of the LDV technique were mentioned in our meeting at Sandia. In the first a holographic lens is employed to prolong the fringe pattern for multiple point measurements. The second is a time of flight measurement which takes advantage of gas breakdown by laser focusing. The emitting plasma follows the flow and is monitored by two detectors which furnish the elapsed time.

The seeding problem poses the greatest difficulty as far as applying the LDV to measurements on board a re-entry vehicle. Particles injected through the wall of the craft would tend to stay close to the wall. Naturally occurring seed however may be present or emitted from the ceramic cover of the re-entry vehicle and these may be used for LDV measurements. The interference fringe detection schemes are more prevalent and easier to use. A very narrow angle α will be required to reduce the count frequency, but this also has the advantage of permitting multiple point measurements.

Thermally excited fluorescence emission and particulate luminosity may mask the signal. For these reasons it seems advisable as a first step to monitor fluorescence and particulate emission. This may be augmented by a laser to determine whether particles exist in the flow. Only after the environmental effects have been documented should an LDV measurement be attemped.

References

I.1 E.F.C. Somerscales, Methods of Experimental Physics, 18A, R.J. Emrich editor (Academic Press, New York, 1981).

I.2 R. Schodl, AGARD Lecture Series No. 90 (1977).

I.3 D.E. Hirleman, Opt. Lett. 3, 19 (1978).

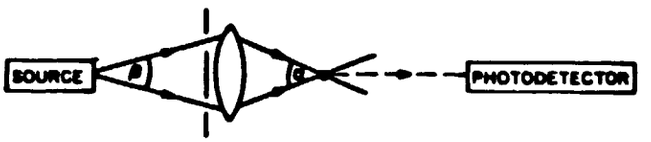

Figure I.1 A Laser Doppler Velocimeter heterodyne detection configuration.

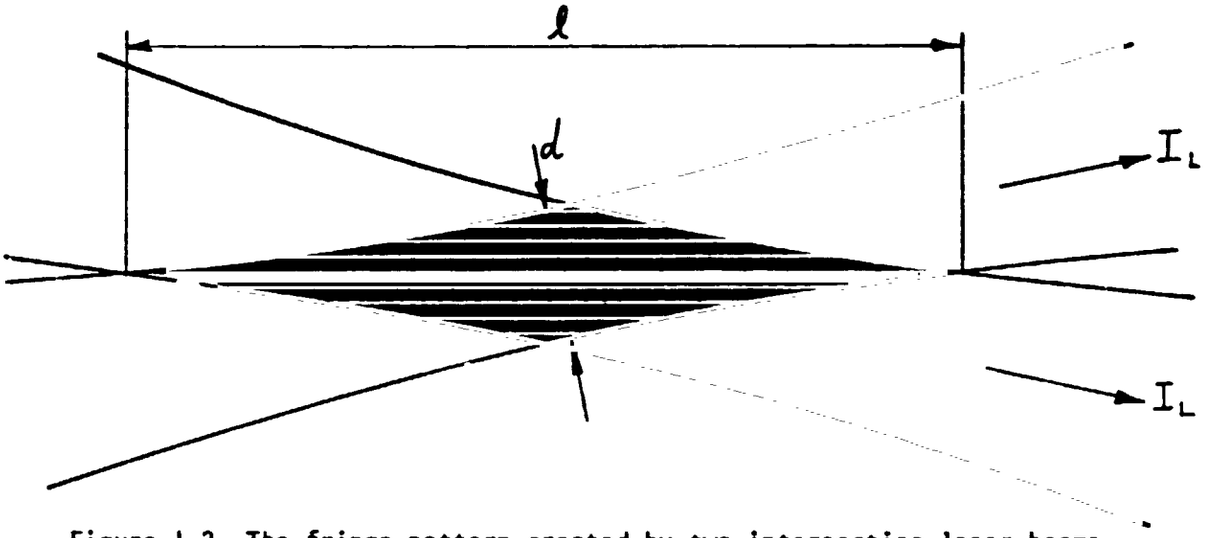

Figure I.2 The fringe pattern created by two intersecting laser beams showing the interaction length ℓ.

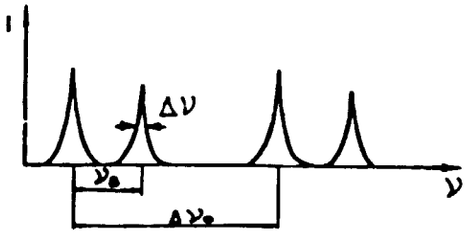

Figure I.3 Fabry Perot output looking at light scattered off particles illuminated by two laser beams.

APPENDIX J. RESONANT DOPPLER VELOCIMETER

The Resonant Doppler Velocimeter (RDV) [J.1] has been used for visualization and for quantitative measurements of velocity, temperature and density of a gaseous flow. These are achieved by shining a single frequency laser beam into a flow which is seeded with an atomic or molecular species. The laser is tuned through the absorption frequency of the seeded species. An optical detector may be configured to monitor fluorescence from any position along the beam to provide good spatial resolution. The velocity is determined by observing the Doppler shift of the absorption frequency. Spectroscopic absorption line broadening mechanisms furnish information regarding the static temperature and density of the moving gas.

The technique has been demonstrated in supersonic and hypersonic flows. Unlike particles needed for the standard laser Doppler velocimeter, tracer atoms injected into the flow follow it closely. But the flow still has to be seeded, a fact which could raise experimental difficulties.

The velocity of the flow is measured by the Doppler shift $\Delta\nu_D$ of the absorption line.

$$\Delta\nu_D = \nu_o \, \hat{k} \, \frac{\vec{U}}{c} \tag{J.1}$$

where ν_o is the absorption frequency in the atomic rest frame, $\hat{k}$ is a unit vector in the direction of the laser beam, $\vec{U}$ is the flow velocity vector and c is the speed of light. The method measures the velocity vector in the direction of the laser beam. A reference has to be furnished to be able to measure the absorption frequency in the atomic rest frame. This can be provided by performing spectroscopy in a stationary gas in a cell or in an atomic beam device.

The temperature and density of the flow give rise to frequency broadening of the spectral line. The temperature effect results in a lineshape which is a Gaussian and the collision frequency, which is directly proportional to density, causes a Lorentzian lineshape. Their combination is a convolution which is known as the Voigt profile. The observed profile may be deconvolved to furnish the separate broadening components. The temperature, T, of the flow is given by

$$T = \left(\frac{\Delta\nu_G \lambda}{2}\right)^2 \frac{M}{2k \ln 2} \tag{J.2}$$

where $\Delta\nu_G$ is the full width at half maximum of the Gaussian lineshape, λ and M are the absorption wavelength and mass of the particular species and k is Boltzmann's constant. The density of the gas, n, is given by

$$n = \frac{\pi \Delta\nu_L}{\sigma \bar{u}} \tag{J.3}$$

where $\Delta\nu_L$ is the full width at half maximum of the Lorentzian lineshape, σ is the collision cross section and $\bar{u}$ is the relative velocity in the center of mass system of the tracer atom and its colliding partner. σ is temperature independent if the hard sphere potential is used. In practice one has to find the temperature dependence of σ by performing a calibration [J.2].

The resonant Doppler velocimeter may also be used for flow field visualization. Regions of higher density in the flow fluoresce more bright. In addition, by tuning the laser to a particular Doppler shifted absorption frequency, one can highlight a particular velocity field.

The many properties which can be measured by using the resonant Doppler velocimeter make it an attractive technique. The major difficulty lies in identifying the proper tracer atom and seeding it into the flow. Sodium atoms have been used in nitrogen and helium flows but sodium would tend to

react with the oxygen existing in the flow field surrounding the vehicle. Sodium does occur naturally in the atmosphere. At the highest altitude of interest (80 km) its concentration of 10^2 cm^{-3} is four orders of magnitude below that used in the laboratory. At lower altitudes its concentration is negligible and the fluorescence signal will be masked by Rayleigh scattering.

Laser induced fluorescence has been demonstrated on N, O and NO suggesting that they could be used as tracers for applying the resonant Doppler velocimeter. The major difficulty is associated with producing a tunable laser system with a narrow linewidth and an output frequency which matches one of the ultraviolet absorption frequencies of the gases present.

References

J.1 M. Zimmermann and R.B. Miles, Appl. Phys. Lett. 37, 885 (1981).

J.2 M. Zimmermann and R.B. Miles, J. Phys. B: At. Mol. Phys. 14, L85 (1981).

$\langle u_i'(x,t)u_i'(x,\hat{t})$ = autocorrelation in the near wall region defined by Eq. 19
$\langle u_i'c'\rangle(x_1)$ = turbulent flux of a passive additive
$u_c(x_1)$ = characteristic velocity appearing in the turbulent model for $\langle u_i'c'\rangle$; $u_c \equiv L(\quad)/T(x_1)$
x = coordinate vector with components x_1, x_2, x_3
$+$ = superscript denoting a quantity made dimensionless using the wall parameters u^* and ν

Greek Letters

α = defined by Eq. 23
δ_c = characteristic size of the concentration layer near the mass transfer interface (Eq. 7)
ν = kinematic viscosity
τ_H = characteristic relaxation time for the velocity autocorrelation in a frame of reference moving with the average velocity
$\langle\tau_M\rangle$ = mean period between burst
Ω = semi-infinite spatial domain

LITERATURE CITED

Abromowitz, M., and I. A. Stegun, *Handbook of Mathematical Functions*, NBS, App. Math Series, 55 (1964)

Berman, N. S., "The Effect of Sample Probe Size on Sublayer Period in Turbulent Boundary Layers," *Chem. Eng. Comm.*, 5, 337 (1980).

Blackwelder, R. F., "The Bursting Process in Turbulent Boundary Layers," *Coherent Structure of Turbulent Boundary Layers*, eds., C. R. Smith and D. E. Abbott, AFOSR, Lehigh Univ., 211 (1978).

Campbell, J. A. and T. J. Hanratty, "A New Theory for Turbulent Mass Transfer at a Solid Boundary," submitted to *A.I.Ch.E. J.* (1981)

Cantwell, B. J., "Organized Motion in Turbulent Flow," *Ann. Rev. Fluid Mech.*, 13, 457 (1981).

Coles, D., "A Model for Flow in the Viscous Sublayer," *Coherent Structure of Turbulent Boundary Layers*, eds., C. R. Smith and D. E. Abbott, AFOSR, Lehigh Univ., 462 (1978).

Kreplin, H. P., and H. Eckelmann, "Behavior of the Three Fluctuating Velocity Components in the Wall Region of a Turbulent Channel Flow," *Phys. Fluids*, 22 (7), 1233 (1979).

Kreplin, H. P., and H. Eckelmann, "Propagation of Perturbations in the Viscous Sublayer and Adjacent Wall Region," *J. Fluid Mech.*, 95, 305 (1979b).

MacLeod, N., and J. W. Purton, "A Model for Turbulent Transfer Processes at a Solid-Fluid Boundary," *Chem. Eng. Sci.*, 32, 483 (1977)

Monin, A. S., and A. M. Yaglom, *Statistical Fluid Mechanics: Mechanics of Turbulence*, 1, MIT Press, Cambridge (1971)

Nakagawa, H., and I. Nezu, "Bursting Phenomenon Near the Wall in Open-Channel Flows and its Simple Mathematical Model," *Memoirs, Fac. Eng.*, Kyoto Univ., 40, 213 (1978).

Petty, C. A., "A Statistical Theory for Mass Transfer Near Interfaces," *Chem. Eng. Sci.*, 30, 413 (1975).

Petty, C. A., and P. E. Wood, "The Effect of Turbulent Mixing on Mass Transfer Near Fluid-Fluid Interfaces for Large Schmidt Numbers," *Chem. Eng. Comm.*, 7, 261 (1980a).

Petty, C. A., and P. E. Wood, "The Effect of Turbulent Mixing on Physicochemical Absorption Near Interfaces," *Chem. Eng. Comm.*, 7, 275 (1980b).

Shaw, D. S., and T. J. Hanratty, "Turbulent Mass Transfer Rates to a Wall for Large Schmidt Numbers," *AIChE J.*, 23, 28 (1977a)

Shaw, D. S., and T. J. Hanratty, "Influence of Schmidt Number on the Fluctuations of Turbulent Mass Transfer to a Wall," *AIChE J.*, 23, 160 (1977b).

Sideman, S., and W. V. Pinczewski, "Turbulent Heat and Mass Transfer at Interfaces: Transport Models and Mechanisms," *Topics in Transport Phenomena*, C. Gutfinger, ed., Hemisphere, 47 (1975).

van Dongen, F. G., A. C. M. Belhaars, and D. A. DeVries, "A Periodic Intermittent Model for the Wall Region of a Turbulent Boundary Layer," *Int. J. Heat Mass Transfer*, 21, 1099 (1978)

Yao, H. T., C. P. Chen, R. W. Snellenberger, P. E. Wood, and C. A. Petty, "The Effect of a Finite Propagation Velocity on Turbulent Mass Transfer Near a Rigid Interface," *Chem. Eng. Comm.*, 12 (1981).

Manuscript received July 27, 1981, revision received November 2, and accepted November 5, 1981

AIAA

Evaluation of a Stochastic Model of Particle Dispersion in a Turbulent Round Jet

J-S. SHUEN, L-D. CHEN and G. M. FAETH

Department of Mechanical Engineering
The Pennsylvania State University
University Park, PA 16802

The accumulation and correlation of data for empirical computations of turbulent particle dispersion is complicated since dispersion is influenced by both particle and turbulence properties. This difficulty can be circumvented by computing dispersion directly, using a stochastic particle dispersion model. The stochastic method requires an estimate of the mean and turbulent properties of the continuous phase. Particle trajectories are then computed using random sampling to determine the instantaneous properties of the continuous phase, similar to a random walk calculation. Mean dispersion properties are obtained by averaging over a statistically significant number of particle trajectories.

Several stochastic particle dispersion models have been proposed. Yuu et al. (1978) use a stochastic dispersion model, which employs empirical correlations of mean and turbulent properties, to analyze their measurements of particle dispersion in jets. Gosman and Ioannides (1981) describe a more comprehensive approach, predicting both flow properties (using a k-ϵ model) and dispersion. The latter procedure is attractive since k-ϵ models yield satisfactory predictions for many of the boundary layer type flows that are encountered with dispersion problems.

The objective of the present investigation was to reexamine the data of Yuu et al. (1978) for particle dispersion in air jets using a stochastic dispersion model similar to Gosman and Ioannides (1981). Shearer et al. (1979) have demonstrated that the present k-ϵ model provides good predictions of existing measurements of mean and turbulent properties within jets. In the following, the present stochastic dispersion model is also calibrated by comparison to predictions by Hinze (1975) and measurements by Snyder and Lumley (1971), for simpler flows, prior to applying the model to the jet dispersion data of Yuu et al. (1978).

Correspondence concerning this paper should be addressed to G. M. Faeth, 214 Mechanical Engineering Building, University Park, PA 16802.

0001-1541-83-6479-0167-$2.00

THEORY

Continuous Phase

Computations of the properties of the continuous phase were only required for the tests of Yuu et al. (1978). The jet dispersion experiments involve a particle laden round air jet injected into still air which can be modeled as a steady axisymmetric boundary layer flow. Particle mass loadings in the jet were 0.1–0.4% which is sufficiently small so that the particles had a negligible effect on mean and turbulent gas-phase properties. Since nozzle exist Mach numbers were less than 0.3, density variations, kinetic energy and viscous dissipation were neglected with little error. Jet Reynolds numbers were 9,500–48,000 which implies that molecular transport can be ignored in comparison to turbulent transport.

Under these assumptions, the governing equations for the continuous phase, including model transport equations for k and ϵ, are:

$$\frac{\partial u}{\partial x} + \frac{1}{r}\frac{\partial}{\partial r}(rv) = D(u) = D(C) = 0 \tag{1}$$

$$D(k) = \mu_t\left(\frac{\partial u}{\partial r}\right)^2 - \rho\epsilon \tag{2}$$

$$D(\epsilon) = C_{\epsilon 1}\mu_t\left(\frac{\epsilon}{k}\right)\left(\frac{\partial u}{\partial r}\right)^2 - C_{\epsilon 2}\frac{\rho\epsilon}{k} \tag{3}$$

where

$$D(\phi) = \rho u\frac{\partial \phi}{\partial x} + \rho v\frac{\partial \phi}{\partial r} - \frac{1}{r}\frac{\partial}{\partial r}\left(r\frac{\mu_t}{\rho_\phi}\frac{\partial \phi}{\partial r}\right) \tag{4}$$

and all dependent variables denote time-averaged quantities. The specification of the boundary conditions for Eqs. 1–4 and their numerical solution is described by Shearer et al. (1979). Solution of these equations yields u,v,C,k and ϵ throughout the flow field.

A conservation equation for particle concentration appears in Eq. 1, assuming that the particles have the same local mean velocity and turbulent diffusivity as the gas phase. This corresponds to the locally homogeneous flow (LHF) approximation for two-phase flows considered by Shearer et al. (1979). LHF calculations were considered since this approximation is frequently invoked. Furthermore, comparing actual dispersion with the LHF limit provides an indication of the effect of the inertial properties of the particles on particle dispersion.

Particle Motion

Particle trajectories were determined using a Lagrangian formulation of the governing equations. Since $\rho_p/\rho > 200$, for the measurements to be considered, it is reasonable to neglect virtual mass, Bassett forces, Magnus forces, etc. Under these assumptions, conservation of momentum yields

$$\frac{du_{pi}'}{dt} = \left(\frac{3\rho C_D}{4d_p\rho_p}\right)(u_i' - u_{pi}')|\vec{u}'' - \vec{u}_p'| + g_i, \quad i = 1,3 \tag{5}$$

where particle motion is based on the instantaneous velocity of the continuous phase. Gravitational forces were negligible for conditions examined by Hinze (1975) and Yuu et al (1979), but are included since the effect was appreciable for the experiments of Snyder and Lumley (1971). The position of the particle was determined from

$$\frac{dx_{pi}'}{dt} = u_{pi}', \qquad i = 1,3 \tag{6}$$

Equations 5 and 6 were numerically integrated using a second-order Runge-Kutta algorithm The trajectories of at least 1,000 particles were computed and averaged to obtain dispersion properties.

Particle Dispersion

Following the method of Gosman and Ioannides (1981) the motion of the particles is tracked as they interact with a succession of turbulent eddies, each of which is assumed to have constant flow properties. Velocity fluctuations were assumed to be isotropic with a Gaussian probability density distribution having a standard deviation of $(2k/3)^{1/2}$ The local distribution is randomly sampled when a particle enters an eddy to obtain the instantaneous velocity as $\vec{u}'' = \vec{u} + \vec{u}'$.

A particle is assumed to interact with an eddy for a time which is the minimum of either the eddy lifetime or the transit time required for the particle to cross the eddy. These times are estimated by assuming that the characteristic size of an eddy is the dissipation length scale, similar to Gosman and Ioannides (1981)

$$L_e = C_\mu^{3/4}k^{3/2}/\epsilon \tag{7}$$

Gosman and Ioannides (1981) compute the eddy lifetime as $t_e = L_e/|\vec{u}'|$, however, we found better agreement with measurements by departing from this particle and employing

$$t_e = L_e/(2k/3)^{1/2} \tag{8}$$

The transit time of a particle was found using the linearized equation of motion for a particle in a uniform flow

$$t_t = -\tau\, ln\,(1 - L_e/(\tau|\vec{u}'' - \vec{u}_p'|)) \tag{9}$$

where $\vec{u}'' - \vec{u}_p'$ is the velocity at the start of the interaction. When $L_e > \tau|\vec{u}'' - \vec{u}_p'|$, the linearized stopping distance of the particle is smaller than the characteristic length scale of the eddy and Eq. 9 has no solution In this case, the eddy has captured the particle and the interaction time is the eddy lifetime.

CALIBRATION OF MODEL

Since the stochastic model involves some rather arbitrary selections of length and time scales, it was calibrated similar to Gosman and Ioannides (1981) using the fundamental dispersion results of Hinze (1975) and Snyder and Lumley (1971). Assuming constant turbulent diffusivity, Hinze (1975) developed an analytical expression for the diffusion of "marked" fluid particles introduced at a constant rate from a point source into a homogeneous isotropic flow. Comparable results for the stochastic model were obtained by fixing u,k and ϵ. The corresponding turbulent diffusivity of the analytical expression was taken as $C_\mu\rho k^2/\epsilon$, which is consistent with

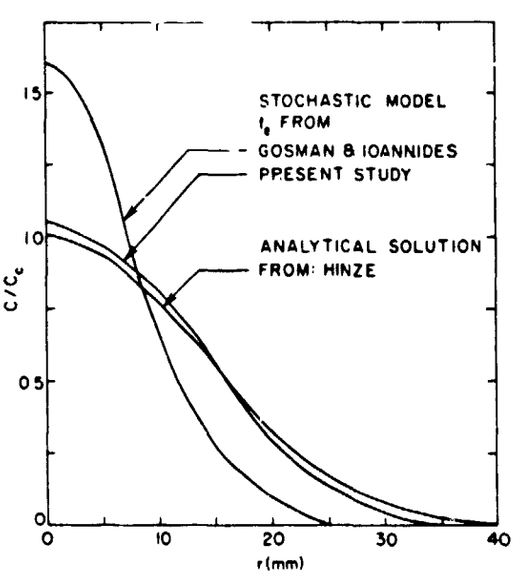

Figure 1. Analytical and stochastic solutions for dispersion of small particles in homogeneous isotropic flow with long diffusion times.

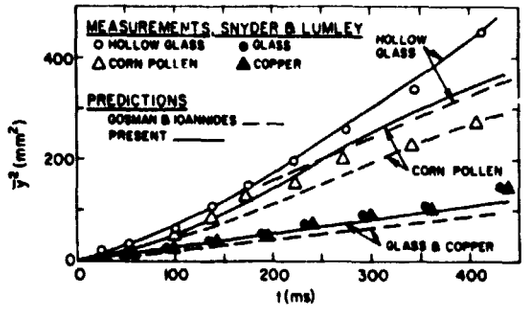

Figure 2. Predicted and measured particle dispersion in a uniform, grid-generated turbulent flow.

the original derivation. The particles were assumed to be small, to correspond with fluid particles. Therefore, the interaction time is always t_e and particle motion is identical to the fluid motion in each eddy.

The radial variation of particle concentration downstream of the point source is illustrated in Figure 1 for the conditions examined by Gosman and Ioannides (1981). Predictions for both stochastic dispersion models are shown, along with the analytical result (C_c was taken from the analytical expression in all cases in order to obtain an absolute comparison). The present stochastic predictions agree favorably with the analytical expression, while the original proposal of Gosman and Ioannides (1981) tends to underestimate the rate of dispersion. (It should be noted that it was not possible to reproduce Gosman and Ioannides (1981) computed results for this flow.)

The second calibration employed the measurements of Snyder and Lumley (1971). These experiments involved the dispersion of individual particles which were isokinetically injected into a uniform turbulent flow downstream of a grid. In this case, interaction times involved both t_e and t_l. The comparison between predictions and measurements is illustrated in Figure 2 The stochastic models provide encouraging agreement with the measurements. The two models yield nearly the same results for heavier particles, where interaction times are mostly fixed by t_l, since this aspect of both models is the same. The present model yields somewhat improved predictions for light particles, where t_e largely controls the interaction time.

PARTICLE LADEN ROUND JET

The experimerts of Yuu et al. (1978) involved an air jet containing nearly monodisperse fly ash particles injected into still air. The nozzle was shaped according to the specifications of Smith and Wang (1944) to yield a uniform outlet velocity. Although Yuu et al. (1978) assumed that gas and particle velocities were identical at the nozzle exit, particle trajectory calculations for the stated nozzle shape indicated that this was not the case. Therefore, particle velocities at the nozzle exit were computed to define initial conditions for the present stochastic dispersion calculations This involved integrating Eq 5 and 6 assuming that particle and gas velocities were identical at the nozzle inlet Gas velocities were determined as a function of distance through the nozzle, assuming frictionless flow for the given nozzle shape and neglecting the small contribution of particle drag on the gas flow properties Computations downstream of the nozzle exit then proceeded as described earlier.

Representative predicted and measured profiles of mean axial gas velocities and particle concentrations are illustrated in Figure 3 The measurements were grouped into ranges of x/d. therefore, predictions are shown for the limits of these ranges Data scatter has been smoothed by only showing mean values for the measurements.

The k-ϵ flow model yields fair predictions of mean gas velocities, particularly in view of the scatter of the data Better performance

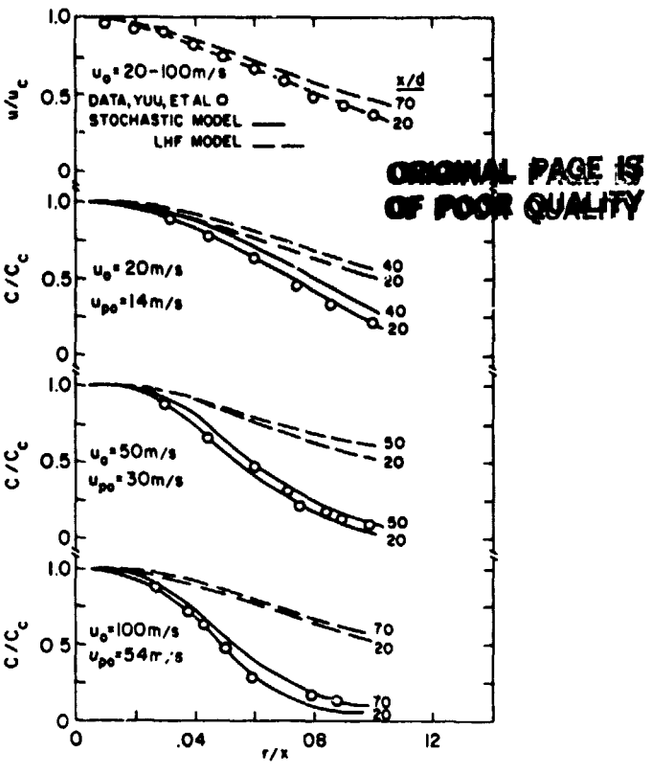

Figure 3. Predicted and measured axial gas velocities and particle concentrations in a dust laden air jet with particle diameter of 20 μm and particle density of 2,000 kg/m³.

of this flow model was generally observed by Shearer et al. (1979) for constant density jets. The stochastic dispersion model, using the computed initial particle velocity, yields quite good agreement with the particle concentration measurements. Similar computations assuming equal particle and gas velocities at the nozzle exit resulted in narrower concentration profiles indicating a significant influence of initial particle conditions on measured dispersion properties. The predictions of the LHF model overestimate the dispersion of particles, therefore, particle inertia is important for these test conditions The particle trajectory computations also yielded significant differences in particle and gas velocities resulting in maximum particle Reynolds numbers on the order of 50

CONCLUSIONS

A stochastic model of particle dispersion by turbulence, proposed by Gosman and Ioannides (1981), has been evaluated The method employs a k-ϵ model to estimate turbulence properties Dispersion is determined by computing particle motion, with random sampling to obtain instantaneous flow properties, for a statistically significant number of particle trajectories

The stochastic model yielded good results, particularly when eddy lifetimes were evaluated using Eq 8 The advantages of the stochastic method are that effects of large relative velocities between the particles and the flow, drag properties at Reynolds numbers greater than the Stokes flow regime, and the variation of local turbulence properties can be readily handled—at least for boundary layer flows.

Additional evaluation of the stochastic model would be desirable Current prescriptions for eddy length and time scales are somewhat arbitrary and further refinement is needed The use of a linear drag law to estimate t_l is suspect for the high particle Reynolds numbers often encountered in practice Finally, while the assumption of isotropic turbulence in the stochastic model is consistent with the

k-ϵ turbulence model, this approximation is questionable for most turbulent flows of interest for dispersion problems.

ACKNOWLEDGMENT

This work was partially supported by NASA Grant No. NAG 3-190, under the technical supervision of R. Tacina of the Lewis Research Center.

NOTATION

C = mean particle concentration
C_D = drag coefficient = $24(1 + Re^{2/3}/6)/Re$, $Re < 1{,}000$; = 0.44, $Re > 1{,}000$
C_i = turbulence model constants: $C_\mu = 0.09$, $C_{\epsilon 1} = 1.44$, $C_{\epsilon 2} = 1.89$
d = nozzle diameter
d_p = particle diameter
g = acceleration of gravity
k = turbulence kinetic energy
L_e = dissipation length scale
r = radial distance
Re = Reynolds number = $\rho|\vec{u}^* - \vec{u}_p^*|d_p/\mu$
t = time
t_e = eddy lifetime
t_t = transit time of particle through eddy
u = mean axial gas velocity
u_i, u_{pi} = gas and particle velocity components
v = mean radial gas velocity
x, x_i = axial distance, component of distance
y = vertical distance

Greek Letters

ϵ = dissipation rate of turbulence kinetic energy
μ = viscosity
μ_t = turbulent viscosity = $C_\mu \rho k^2/\epsilon$
ρ = density
σ_ϕ = turbulent Prandtl/Schmidt numbers: $\sigma_{u_i} = \sigma_k = 1$, $\sigma_\epsilon = 1.3$, $\sigma_C = 0.7$
τ = particle relaxation time = $4\rho_p d_p/(3\rho C_D|\vec{u} - \vec{u}_p|)$
ϕ = generic property

Subscripts

c = centerline value
i = component in direction i
p = particle property
o = initial condition

Superscripts

$(\vec{\ })$ = vector quantity
$(\bar{\ })$ = mean quantity
$(')$ = fluctuation with respect to mean quantity
$(^*)$ = instantaneous value

LITERATURE CITED

Gosman, A. D., and E. Ioannides, "Aspects of Computer Simulation of Liquid-Fueled Combustors," *AIAA Paper*, No. 81-0323 (1981).

Hinze, J. O., *Turbulence*, 2nd ed., McGraw-Hill, New York (1975).

Shearer, A. J., H. Tamura, and G. M. Faeth, "Evaluation of a Locally Homogeneous Flow Model of Spray Evaporation," *J. of Energy*, 3, 271 (1979).

Smith, R. H., and C.-T. Wang, "Contracting Cones Giving Uniform Throat Speeds," *J. Aero. Sci.*, 11, 356 (1944).

Snyder, W. H., and J. L. Lumley, "Some Measurements of Particle Velocity Autocorrelation Functions in a Turbulent Flow," *J. Fluid Mech.*, 48, 41 (1971).

Yuu, S., N. Yasukouchi, Y. Hirosawa, and T. Jotaki, "Particle Turbulent Diffusion in a Dust Laden Round Jet," *AIChE J.*, 24, 509 (1978).

Manuscript received September 17, 1981, revision received December 11, and accepted January 13, 1982.